
This is an electronic reprint of the original article.
This reprint may differ from the original in pagination and typographic detail.

Menczel, Paul; Pyhäranta, Tuomas; Flindt, Christian; Brandner, Kay

Two-stroke optimization scheme for mesoscopic refrigerators

Published in:
Physical Review B

DOI:
[10.1103/PhysRevB.99.224306](https://doi.org/10.1103/PhysRevB.99.224306)

Published: 21/06/2019

Document Version
Publisher's PDF, also known as Version of record

Please cite the original version:
Menczel, P., Pyhäranta, T., Flindt, C., & Brandner, K. (2019). Two-stroke optimization scheme for mesoscopic refrigerators. *Physical Review B*, 99(22), 1-16. Article 224306. <https://doi.org/10.1103/PhysRevB.99.224306>

This material is protected by copyright and other intellectual property rights, and duplication or sale of all or part of any of the repository collections is not permitted, except that material may be duplicated by you for your research use or educational purposes in electronic or print form. You must obtain permission for any other use. Electronic or print copies may not be offered, whether for sale or otherwise to anyone who is not an authorised user.

Two-stroke optimization scheme for mesoscopic refrigerators

Paul Menczel, Tuomas Pyhäranta, Christian Flindt, and Kay Brandner
Department of Applied Physics, Aalto University, 00076 Aalto, Finland

 (Received 2 April 2019; revised manuscript received 7 June 2019; published 21 June 2019)

Refrigerators use a thermodynamic cycle to move thermal energy from a cold reservoir to a hot one. Implementing this operation principle with mesoscopic components has recently emerged as a promising strategy to control heat currents in micro and nanosystems for quantum technological applications. Here we combine concepts from stochastic and quantum thermodynamics with advanced methods of optimal control theory to develop a universal optimization scheme for such small-scale refrigerators. Covering both the classical and the quantum regime, our theoretical framework provides a rigorous procedure to determine the periodic driving protocols that maximize either cooling power or efficiency. As a main technical tool, we decompose the cooling cycle into two strokes, which can be optimized one by one. In the regimes of slow or fast driving, we show how this procedure can be simplified significantly by invoking suitable approximations. To demonstrate the practical viability of our scheme, we determine the exact optimal driving protocols for a quantum microcooler, which can be realized experimentally with current technology. Our work provides a powerful tool to develop optimal design strategies for engineered cooling devices and it creates a versatile framework for theoretical investigations exploring the fundamental performance limits of mesoscopic thermal machines.

DOI: [10.1103/PhysRevB.99.224306](https://doi.org/10.1103/PhysRevB.99.224306)

I. INTRODUCTION

With the rapid advance of quantum technologies during the last decade, the search for new strategies to overcome the challenges of thermal management at low temperatures and small length scales has become a subject of intense research [1–5]. Solid-state quantum devices based on, for example, superconducting circuits require operation temperatures in the range of milli-Kelvins, which must currently be upheld with massive and costly cryogenic equipment. These systems are among the most promising candidates to realize a large-scale quantum computer [6–8]; they also provide a versatile platform for the design of accurately tunable thermal instruments that can be implemented on chip and thus make it possible to control the heat flow between individual components of complex quantum circuits [9–16]. This technology could significantly simplify the operation of quantum devices by enabling the selective cooling of their functional degrees of freedom.

Nanoscale refrigerators play a promising role in the development of integrated quantum cooling solutions. Mimicking the cyclic operation principle of their macroscopic counterparts, which are used in everyday appliances such as freezers and air conditioners, these mesoscopic machines use periodic driving fields to transfer heat from a cold object to a hot one [17–28]. In contrast to continuously operating thermal devices, like the ones considered in Refs. [29–31], such cyclic refrigerators do not require a constant flow of matter and are therefore arguably easier to combine with other components of complex quantum circuits. Their basic working mechanism can be understood as a two-stroke process. In the first stroke, a certain amount of heat is absorbed from the cold body into a working system, which acts as a container for thermal energy. The second stroke uses the power input from the external driving field to inject the acquired heat into a hot reservoir and

restore the initial state of the working system as illustrated in Fig. 1.

The thermodynamic performance of this cycle is crucially determined by the driving protocol that is applied to the working system. Finding its optimal shape is vital for practical applications and, at the same time, constitutes a formidable theoretical task. In fact, finding optimal strategies to control periodic thermodynamic processes in small-scale systems is a longstanding problem in both stochastic [32–42] and quantum

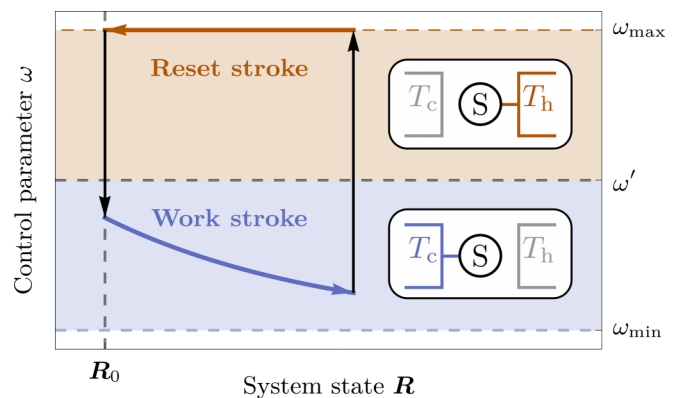


FIG. 1. Thermodynamic operation cycle of a two-stroke refrigerator. Depending on whether the value of the control parameter ω is smaller or larger than a given threshold ω' , the working system S couples to a reservoir with temperature T_c or to a hotter one with temperature $T_h > T_c$. The possible values of the control parameter are delimited by ω_{\min} and ω_{\max} . In the work stroke, heat is transferred from the cold reservoir to the working system (blue arrow). The reset stroke restores the initial state R_0 , while S is in contact with the hot reservoir (red arrow). The two strokes are connected by instantaneous jumps of the control parameter (black arrows).

thermodynamics [43–48], which involves three major challenges. First, the intricate interdependence between state and control variables that governs the dynamics of mesoscopic devices leads to constraints that can usually not be solved explicitly. Second, thermodynamic figures of merit such as cooling power are typically unbounded functions of external control parameters. The optimal protocol is then determined by the boundaries of the admissible parameter space and cannot be found from Euler-Lagrange equations, a situation known as a bang-bang scenario [49–51]. Third, a periodic mode of operation requires that the initial configuration of the device is restored after a given cycle time [47,52]. This constraint effectively renders the optimization problem nonlocal in time, since any change of the driving protocol during the cycle affects the final state of the working system.

In this article we show how these problems can be handled in three successive steps forming a universal scheme that makes it possible to maximize both the cooling power and the efficiency of mesoscopic refrigerators. The key idea of our method is to divide the refrigeration cycle into two strokes, which can be optimized one by one after fixing suitable boundary conditions, see Fig. 1. Dynamical constraints are thereby included through time-dependent Lagrange multipliers and bang-bang type protocols are taken into account systematically by applying Pontryagin’s minimum principle [49,53] as we explain in the following. This two-step procedure effectively fixes the shape of the optimal driving protocol. The extracted heat, which initially depends on the entire control protocol, is thus reduced to an ordinary function of time-independent variational parameters, which can be optimized with standard techniques.

To illustrate our general formalism, we analyze a semiclassical model of a realistic quantum microcooler based on superconducting circuits, which can be implemented with current experimental technology [16,45]. This application demonstrates the practical viability of our new scheme. Moreover, since the optimization of our model can be performed essentially through analytical calculations, it also provides valuable insights into characteristic features of optimal cooling cycles in mesoscopic systems.

The scope of our two-stroke framework is not limited to elementary models that can be treated exactly. By contrast, owing to its general structure, our scheme can be combined with a variety of established dynamical approximation methods to become an even more powerful theoretical tool. In this way, a physically transparent picture can also be obtained of complicated optimization problems, for which even numerically exact solutions would be practically out of reach. In the second part of our paper, we show how such a perturbative approach can be implemented for the limiting regimes of slow and fast driving. We round off our work by applying these techniques to determine the optimal working conditions of a superconducting microcooler in the full quantum regime.

Our paper is organized as follows. In Sec. II we establish our two-stroke optimization scheme, which provides the general basis for this paper. In Sec. III we use this framework to optimize the performance of a realistic model for a quantum microcooler in the semiclassical regime. We further develop our general theory in Sec. IV by incorporating two key dynamical approximation methods. In Sec. V we apply these

techniques to extend the semiclassical case study of Sec. III to the coherent regime. Finally, we conclude and discuss the new perspectives opened by our work in Sec. VI. Appendices A and B contain further technical details of our calculations.

II. GENERAL SCHEME

A. Setup

A two-stroke refrigerator consists of three basic components: Two reservoirs at different temperatures T_c and $T_h > T_c$ and a controlled working system [31,54]. We start by developing our general scheme before moving on to specific applications in Secs. III and V. The internal state of the working system is described by a vector of N independent variables \mathbf{R}_t , which follows the time evolution equation

$$\dot{\mathbf{R}}_t = \mathbf{F}[\mathbf{R}_t, \omega_t], \quad (1)$$

with dots indicating time derivatives throughout. The generator \mathbf{F} thereby depends on the specific architecture of the device and it is assumed to be local in time, i.e., it only depends on the state vector \mathbf{R}_t and the driving protocol ω_t at time t . It may, however, be a nonlinear function of these variables. The external parameter ω_t plays a threefold role; it controls the dynamics of the state vector, modulates the internal energy landscape of the working system, and it regulates the coupling to the reservoirs [55].

The key idea of our two-stroke scheme is to disentangle these effects. To this end, we assume that the working system is connected either to the cold or the hot reservoir depending on whether ω_t is smaller or larger than a given threshold value ω' . A thermodynamic cooling cycle can then be realized as illustrated in Fig. 1. In the work stroke, the control parameter ω_t changes continuously and does not exceed the threshold ω' . Thus, the working system is constantly coupled to the cold reservoir, from which it has picked up the heat

$$\mathcal{Q}_c[\omega_t] \equiv \int_0^{\tau'} J[\mathbf{R}_t, \omega_t] dt \quad (2)$$

by the end of the stroke. Here $J[\mathbf{R}_t, \omega_t]$ is the instantaneous heat flux flowing into the system. Throughout this paper, we use calligraphic letters to denote functionals, which depend on the complete driving protocol ω_t , for example the left-hand side of (2). At the switching time τ' , ω_t is abruptly raised above the threshold ω' . This operation initializes the reset stroke, during which the control parameter follows a continuous trajectory without falling below ω' . Hence, the system is coupled to the hot reservoir throughout this stroke, which restores the initial state of the system and releases the heat

$$\mathcal{Q}_h[\omega_t] \equiv - \int_{\tau'}^{\tau} J[\mathbf{R}_t, \omega_t] dt. \quad (3)$$

The cycle is completed at the time τ by instantaneously resetting the control parameter to its initial value.

The specific form of the function $J[\mathbf{R}_t, \omega_t]$ is determined by the architecture of the refrigerator. For example, if the working system can be described as an open quantum system in the weak coupling regime, this quantity can universally be identified as [56–59]

$$J[\mathbf{R}_t, \omega_t] \equiv \text{tr}[H_t \dot{\rho}_t]. \quad (4)$$

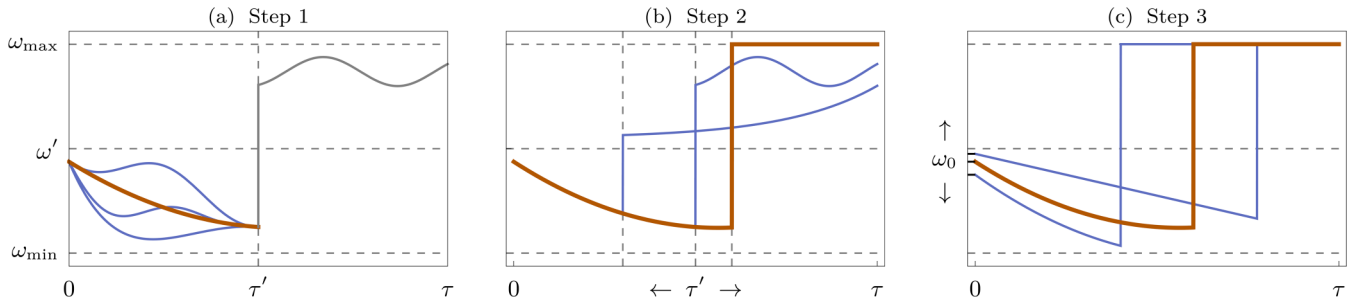


FIG. 2. Maximizing the cooling power of a two-stroke refrigerator in three steps. (a) In step 1, the optimal work protocol (red line) is determined by variation of the functional (5) for a fixed switching time τ' . Adding small displacements (blue lines) to the optimal protocol can only reduce the extracted heat. The reset stroke protocol (gray line) does not play a role here. (b) Step 2 optimizes the reset protocol such that the initial state of the system is restored, while keeping the optimal work stroke with given initial conditions fixed. The optimal reset stroke (in red) is thereby distinguished by having the latest possible switching time τ' . The blue lines are examples of nonoptimal reset stroke protocols with earlier switching times. (c) The initial values are determined in step 3, which completes the optimal protocol (in red). It is here compared to the protocols in blue, which are obtained by following steps 1 and 2 for different initial conditions and yield a lower heat extraction.

Here $H_t \equiv H[\omega_t]$ denotes the Hamiltonian of the working system and $\rho_t \equiv \rho[\mathbf{R}_t]$ is the density matrix describing its state. Remarkably, our two-stroke scheme enables a general optimization procedure even without such specifications, as we will show in the following.

B. Maximum heat extraction

Our first aim is to find the control protocol ω_t^p that maximizes the heat extraction (2) for a given cycle time τ . To this end we proceed along the three steps illustrated in Fig. 2.

First, for the optimal work stroke, ω_t has to be chosen such that the extended objective functional for the extracted heat

$$\mathcal{Q}_c[\mathbf{R}_t, \lambda_t, \omega_t] \equiv \int_0^{\tau'} \{J[\mathbf{R}_t, \omega_t] - \lambda_t \cdot (\dot{\mathbf{R}}_t - \mathbf{F}[\mathbf{R}_t, \omega_t])\} dt \quad (5)$$

becomes stationary, i.e., its functional derivative with respect to its arguments vanishes [49]. Here we have introduced a vector of Lagrange multipliers λ_t to account for the dynamical constraint (1). This extension of the parameter space makes it possible to treat the control parameter ω_t and the state \mathbf{R}_t as independent variables. Optimizing the functional (5) is formally equivalent to applying the least-action principle in Hamiltonian mechanics with \mathbf{R}_t and λ_t playing the role of generalized coordinates and canonical momenta, respectively [60]. The corresponding effective Hamiltonian is given by

$$H_w[\mathbf{R}_t, \lambda_t, \omega_t] \equiv J[\mathbf{R}_t, \omega_t] + \lambda_t \cdot \mathbf{F}[\mathbf{R}_t, \omega_t]. \quad (6)$$

Thus, after fixing the initial conditions $\mathbf{R}_{t=0} = \mathbf{R}_0$ and $\lambda_{t=0} = \lambda_0$, the optimal protocol for the work stroke is uniquely determined by the canonical equations [49]

$$\dot{\mathbf{R}}_t = \frac{\partial H_w}{\partial \lambda_t}, \quad \dot{\lambda}_t = -\frac{\partial H_w}{\partial \mathbf{R}_t}, \quad \text{and} \quad \frac{\partial H_w}{\partial \omega_t} = 0. \quad (7)$$

Note that the last equation is purely algebraic. Therefore, the initial value of the control parameter ω_0 is fixed by choosing \mathbf{R}_0 and λ_0 .

Second, since only the work stroke contributes to the extracted heat, the optimal reset stroke minimizes the reset time $\mathcal{T}_r \equiv \tau - \tau'$, during which the system returns to its initial state. To implement this condition, we have to minimize the

extended objective functional for the reset time

$$\begin{aligned} \mathcal{T}_r[\mathbf{R}_t, \lambda_t, \omega_t] &\equiv \int_{\tau'}^{\tau} \{1 - \lambda_t \cdot (\dot{\mathbf{R}}_t - \mathbf{F}[\mathbf{R}_t, \omega_t])\} dt \\ &\equiv \int_{\tau'}^{\tau} (H_r[\mathbf{R}_t, \lambda_t, \omega_t] - \lambda_t \cdot \dot{\mathbf{R}}_t) dt, \end{aligned} \quad (8)$$

with respect to the dynamical variables \mathbf{R}_t , λ_t , and ω_t , and the switching time τ' . Thus, the optimal reset protocol can be found by solving the canonical equations

$$\dot{\mathbf{R}}_t = \frac{\partial H_r}{\partial \lambda_t}, \quad \dot{\lambda}_t = -\frac{\partial H_r}{\partial \mathbf{R}_t}, \quad \text{and} \quad \frac{\partial H_r}{\partial \omega_t} = 0, \quad (9)$$

with respect to the boundary conditions

$$\begin{aligned} \mathbf{R}_{t=\tau'} &= \mathbf{R}'[\mathbf{R}_0, \lambda_0], \quad \mathbf{R}_{t=\tau} = \mathbf{R}_0, \quad \text{and} \\ H_r[\mathbf{R}_{\tau'}, \lambda_{\tau'}, \omega_{\tau'}] &= 0. \end{aligned} \quad (10)$$

Here \mathbf{R}' is the state vector of the system after the optimal work stroke, and the end-point condition $\mathbf{R}_{t=\tau} = \mathbf{R}_0$ replaces the initial condition for the Lagrange multipliers.

Note that the state \mathbf{R}_t has to be continuous throughout the cycle [33,61], while the Lagrange multipliers λ_t of the work and reset strokes are independent variables; they therefore do not have to satisfy any boundary conditions. The last requirement in (10) minimizes \mathcal{T}_r with respect to the initial time τ' [49]. In practice, the switching time τ' and the initial Lagrange multipliers $\lambda_{\tau'}$ have to be determined together such that the conditions (10) are satisfied.

The procedure above leads to the optimal protocol if the algebraic condition $\partial_{\omega_t} H_r = 0$ can be satisfied throughout the reset stroke. However, the reset Hamiltonian H_r does often not have a local extremum within the admissible range $[\omega', \omega_{\max}]$ of the control parameter [47,51]. The optimal reset protocol ω_t^p then has to assume one of the boundary values ω' or ω_{\max} , so that it minimizes the effective Hamiltonian H_r . Formally, we thus replace the last equation in (9) by the more general requirement

$$H_r[\mathbf{R}_t^p, \lambda_t^p, \omega_t^p] \leq H_r[\mathbf{R}_t^p, \lambda_t^p, \omega], \quad (11)$$

which is also known as Pontryagin's minimum principle [49,53]. Here \mathbf{R}_t^p and λ_t^p are the optimal trajectories of the state vector and the Lagrange multiplier, respectively. The

canonical equations (9) can thus be integrated as follows. First, for given initial conditions \mathbf{R}_0 and λ_0 , the initial value of the control parameter ω_0 has to be determined such that $H_r[\mathbf{R}_0, \lambda_0, \omega_0]$ becomes minimal. If this function does not have a local minimum within the range $[\omega', \omega_{\max}]$, we either have $\omega_0 = \omega'$ or $\omega_0 = \omega_{\max}$. After fixing ω_0 , the state vector and the Lagrange multipliers can be propagated for a short time dt using the canonical equations. The control parameter is then updated by minimizing the Hamiltonian $H_r[\mathbf{R}_{dt}, \lambda_{dt}, \omega_{dt}]$ with respect to ω_{dt} . Iterating this procedure until the final time τ yields the optimal trajectories \mathbf{R}_t^p , λ_t^p , and ω_t^p . This prescription typically leads to protocols that are either constant or consist of constant pieces connected by continuous trajectories [50]. In Sec. III we will show how both of these cases can be handled in practice.

Third and finally, after completing steps 1 and 2, we arrive at the optimal protocol $\omega_t^p = \omega_t^p[\mathbf{R}_0, \lambda_0]$ for fixed initial conditions \mathbf{R}_0 and λ_0 . Inserting this solution into (2) renders the extracted heat an ordinary function of $2N$ variables $Q_c = Q_c[\mathbf{R}_0, \lambda_0]$. The last step of our scheme thus consists of maximizing this function over the state space of the working system and the set of admissible Lagrange multipliers, i.e., those λ_0 , for which $\omega_0 = \omega_0[\mathbf{R}_0, \lambda_0]$ falls into the permitted range $[\omega_{\min}, \omega']$. We note that maximizing Q_c over all initial conditions \mathbf{R}_0 and λ_0 is equivalent to maximizing Q_c over all switching times τ' and all boundary values \mathbf{R}_0 and \mathbf{R}' , since these quantities are connected by a one-to-one mapping.

C. Maximum efficiency

So far we have developed a scheme to maximize the extracted heat per operation cycle of a general two-stroke refrigerator. A thorough optimization of a thermal machine, however, also has to take into account the consumed input, which, for a cooling device, corresponds to the work $\mathcal{W}[\omega_t]$ that the external controller has to supply to drive the heat flux. To this end, we now show how to find the optimal protocol ω_t^j , which maximizes the efficiency

$$\begin{aligned} \eta[\omega_t] &\equiv Q_c[\omega_t]/\mathcal{W}[\omega_t] \\ &= Q_c[\omega_t]/(Q_h[\omega_t] - Q_c[\omega_t]), \end{aligned} \quad (12)$$

also referred to as ‘‘coefficient of performance’’ [54]. Note that here we have used the first law of thermodynamics to express the work input $\mathcal{W}[\omega_t]$ in terms of the released and the extracted heat $Q_h[\omega_t]$ and $Q_c[\omega_t]$. Owing to the second law, the figure of merit (12) is subject to the Carnot bound

$$\eta[\omega_t] \leq \eta_C \equiv \frac{T_c}{T_h - T_c}, \quad (13)$$

which is saturated in the reversible limit at the price of vanishing cooling power [18]. Hence, for a practical optimization criterion, we have to fix both the cycle time τ and the heat extraction $Q_c[\omega_t] = Q_c^*$. Maximizing the efficiency (12) then amounts to minimizing the effective input $Q_h[\omega_t]$, i.e., the average heat injected into the hot reservoir per operation cycle.

The corresponding protocol $\omega_t^j = \omega_t^j[Q_c^*]$ renders the work stroke as short as possible such that the maximum amount of time is left to reduce the heat release in the reset stroke [62].

Hence, in the first step, we have to minimize the working time

$$\begin{aligned} \mathcal{T}_w[\mathbf{R}_t, \lambda_t, \omega_t, \mu] \\ \equiv \int_0^{\tau'} \{1 - \mu(Q_c^* + \lambda_t \cdot \dot{\mathbf{R}}_t - H_w[\mathbf{R}_t, \lambda_t, \omega_t])\} dt, \end{aligned} \quad (14)$$

where the time-independent Lagrange multiplier μ has been introduced to fix the total heat extraction Q_c^* . This variational problem again leads to the canonical equations (7), which have to be solved for given initial conditions \mathbf{R}_0 and λ_0 to find the optimal work protocol. In fact, this protocol also maximizes the heat extraction for every given time t , i.e., we have $\omega_t^j[\mathbf{R}_0, \lambda_0] = \omega_t^p[\mathbf{R}_0, \lambda_0]$ during the work stroke. However, the switching time $\tau' = \tau'[\mathbf{R}_0, \lambda_0, Q_c^*]$ now has to be chosen such that the constraint

$$\int_0^{\tau'} J[\mathbf{R}_t, \omega_t] dt = Q_c^* \quad (15)$$

is satisfied. Hence, the switching time is now determined by the work stroke rather than the reset stroke.

After completing step 1, the optimal reset protocol is found by minimizing the functional

$$Q_h[\mathbf{R}_t, \lambda_t, \omega_t] \equiv \int_{\tau'}^{\tau} \{-J[\mathbf{R}_t, \omega_t] - \lambda_t \cdot (\dot{\mathbf{R}}_t - \mathbf{F}[\mathbf{R}_t, \omega_t])\} dt \quad (16)$$

for the boundary conditions

$$\mathbf{R}_{t=\tau'} = \mathbf{R}'[\mathbf{R}_0, \lambda_0, Q_c^*] \quad \text{and} \quad \mathbf{R}_{t=\tau} = \mathbf{R}_0. \quad (17)$$

This problem will, depending on the initial conditions, only admit a proper solution if the device can actually produce the cooling power Q_c^*/τ in a cyclic mode of operation. It might therefore be helpful to introduce an intermediate step, which decides whether or not the cycle can be closed for the boundary conditions (17). To solve the canonical equations for the objective functional (16), it might again be necessary to invoke Pontryagin’s minimum principle, as we will demonstrate explicitly in Sec. III D.

Once the reset protocol has been determined, the efficiency (12) can be reduced to an ordinary function of \mathbf{R}_0 and λ_0 . Maximizing this function under the constraint $\omega_0[\mathbf{R}_0, \lambda_0] \in [\omega_{\min}, \omega']$ yields the maximal-efficiency protocol $\omega_t^j[Q_c^*]$. Note that the set of admissible initial conditions is thereby also restricted by fixing the heat extraction Q_c^* .

D. Discussion

Before moving on to practical applications of the optimization scheme developed in this section, it is instructive to briefly discuss the two key conditions that our method relies on. First, it is tailored for situations where the energy landscape of the cooling device and its interaction with the external reservoirs are controlled through a single driving parameter. Second, it requires that the working system fully decouples from one of the reservoirs in both strokes. Once these two assumptions are met, our scheme can be used for most common setups of quantum engineering such as arbitrary complex multilevel systems in the weak-coupling limit. Moreover, it might even be applied in the strong-coupling regime, provided that the dynamics of the working

system can still be described with a time-local generator of the form (1) and that the heat functionals (2) and (3) can be properly identified. This perspective is particularly interesting, since the potential advantages of strongly coupled thermal machines are currently subject of an active debate in quantum thermodynamics, see for example [63–65].

Finally, we would like to point out that the assumption of perfect decoupling, which might at first seem quite restrictive but is often well justified in practice [45], can in principle be relaxed. In fact, our three-step procedure can still be applied as described above even if the dynamics of the working system is affected by both reservoirs throughout the cycle. It would then no longer yield the formally exact optimal protocol but still a good approximation, provided that the dominant amount of heat in each of the two strokes is exchanged either with the hot or the cold reservoir. Whether or not this modification improves the overall quality of the optimization depends on the properties of the specific system and must be assessed on a case-by-case basis.

III. QUANTUM MICROCOOLER I: SEMICLASSICAL REGIME

A. System

We will now show how our general theory can be applied to a concrete problem of quantum engineering. Specifically, we optimize the performance of a quantum microcooler, which can be implemented with superconducting components, see Fig. 3(a). The core of this device is an engineered two-level system with Hamiltonian [18]

$$H_t \equiv \frac{\hbar\Delta}{2}\sigma_x + \frac{\hbar\omega_t}{2}\sigma_z. \quad (18)$$

Here \hbar denotes the reduced Planck constant, σ_x and σ_z are Pauli matrices, Δ corresponds to the device-specific tunneling energy, and ω_t is the tunable energy bias, which plays the role of the external control parameter. This system is embedded in an electronic circuit, which couples it either to a cold or a hot reservoir depending on the value of ω_t . Thus, applying a suitable periodic control protocol ω_t makes it possible to realize a two-stroke cooling cycle, as illustrated in Fig. 3(b).

B. Step-rate model

For a quantitative description of the microcooler, we consider the model shown in Fig. 3(a), which makes it possible to determine the optimal control protocol analytically. To this end, we here focus on the semiclassical limit, where the tunneling energy Δ is negligible and the Hamiltonian commutes with itself at different times. The periodic density matrix of the working system is then fully determined by the level populations and can be parametrized as

$$\rho_t \equiv \frac{1}{2}(1 + R_t \sigma_z). \quad (19)$$

The state variable R_t thereby obeys the Bloch equation [58]

$$\begin{aligned} \dot{R}_t &= F[R_t, \omega_t] \equiv -\Gamma^+[\omega_t] R_t - \Gamma^- [\omega_t] \quad \text{with} \\ \Gamma^\pm [\omega_t] &\equiv \gamma [\omega_t] (1 \pm \exp[-\hbar\omega_t/T[\omega_t]]). \end{aligned} \quad (20)$$

Here the Boltzmann factors appear due to the detailed balance condition, which fixes the relative frequency of thermal

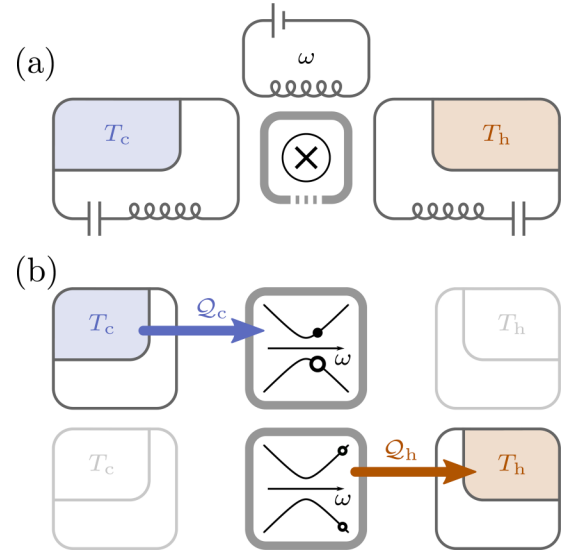


FIG. 3. Quantum microcooler. (a) Sketch of the experimental setup described in Refs. [16,18,45]. A superconducting qubit is coupled to two resonant circuits with different resonance frequencies. Each circuit contains a metallic island acting as a mesoscopic reservoir with temperature T_c and $T_h > T_c$, respectively. An additional bias circuit is used to control the level splitting of the qubit by varying the applied magnetic flux. (b) Scheme of the thermodynamic cooling cycle. The two central diagrams show the energy levels of the qubit as a function of the external bias ω and the corresponding populations at the beginning of each stroke. By the end of the work stroke, the qubit has picked up the heat Q_c from the cold island. The level splitting is then instantaneously increased to tune the qubit into resonance with the hot island. During the following reset stroke, the initial level populations are restored, while the heat Q_h flows into the hot reservoir. The cycle is completed by setting the level splitting back to its initial value, thus reconnecting the qubit to the cold island.

excitation and relaxation events [54]. The corresponding temperature is determined by the reservoir coupled to the system, i.e.,

$$T[\omega \leq \omega'] \equiv T_c \quad \text{and} \quad T[\omega > \omega'] \equiv T_h, \quad (21)$$

where ω' corresponds to the threshold energy of the device. Note that Boltzmann's constant is set to 1 throughout. The factor $\gamma[\omega]$ in (20) accounts for the finite energy range of the coupling mechanism between working system and reservoirs, which depends on the specific design of the circuit. For the sake of simplicity, we here use an idealized model, where the rates (20) feature a step-type dependence on ω , i.e., we set

$$\gamma[\omega] \equiv \gamma = \text{const for } 0 < \omega \leq \omega_{\text{max}} \quad (22)$$

and $\gamma[\omega] \equiv 0$ otherwise. Hence, the two-level system is decoupled from its environment if ω falls outside its admissible range. Note that we have set ω_{min} to zero.

Under weak-coupling conditions, the instantaneous heat flux into the qubit is given by (4). The average amount of heat that the microcooler extracts from the cold reservoir in one cycle of duration τ then becomes

$$Q_c[\omega_t] \equiv \int_0^\tau \frac{\hbar\omega_t}{2} \dot{R}_t dt = \int_0^\tau \frac{\hbar\omega_t}{2} F[R_t, \omega_t] dt, \quad (23)$$

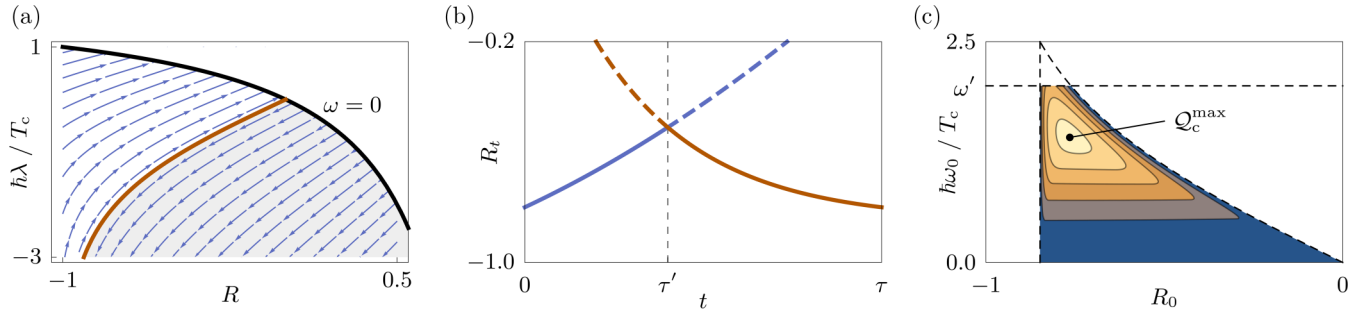


FIG. 4. Maximizing the cooling power of a quantum microcooler in three steps. (a) The plot shows the flow of the effective Hamiltonian vector field (28), which determines the optimal dynamics of the system during the work stroke. The black line marks the boundary of the physical region of the effective phase space, where the level splitting ω is positive. The red line separates solutions with positive (unshaded) and negative (shaded) cooling power. (b) The state trajectories during the optimal work and reset stroke, (31) and (36), are plotted in blue and red, respectively, for typical initial conditions. Their intersection point determines the optimal switching time τ' . The solid line shows the combined optimal state trajectory, which excludes the dashed parts. (c) The maximum heat extraction $Q_c[R_0, \omega_0]$ is plotted over the admissible range (37) of initial conditions, which is bounded by the dashed black curves corresponding to $R_0 = -\tanh[\hbar\omega_0/(2T_c)]$, $R_0 = -\tanh[\hbar\omega_{\max}/(2T_h)]$ and $\omega_0 = \omega'$. Brighter colors indicate a larger amount of extracted heat. The global maximum Q_c^{\max} is shown with a dot. All panels were created with the parameter values $\omega' = 2T_c/\hbar$, $\omega_{\max} = 5T_c/\hbar$, $T_h = 2T_c$, and $\tau = 3/\gamma$.

where $\tau' \in [0, \tau]$ denotes the length of the work stroke. Accordingly, the average heat injected into the hot reservoir is given by

$$Q_h[\omega_t] \equiv - \int_{\tau'}^{\tau} \frac{\hbar\omega_t}{2} F[R_t, \omega_t] dt. \quad (24)$$

C. Maximum heat extraction

The extracted heat (23) can be maximized using the general scheme of Sec. II B. To this end, we first have to determine the optimal work stroke, which is described by the effective Hamiltonian [66]

$$H_w[R_t, \lambda_t, \omega_t] = -(\omega_t + \lambda_t)(\Gamma^+[\omega_t] R_t + \Gamma^-[\omega_t]). \quad (25)$$

The corresponding canonical equations follow from (7) and are given by

$$\begin{aligned} \dot{R}_t &= -\Gamma^+[\omega_t] R_t - \Gamma^-[\omega_t], \\ \dot{\lambda}_t &= \Gamma^+[\omega_t](\omega_t + \lambda_t), \quad \text{and} \\ \omega_t &= (T_c/\hbar) - \lambda_t - (T_c/\hbar) W_0 \left[e^{1-\hbar\lambda_t/T_c} \frac{1+R_t}{1-R_t} \right], \end{aligned} \quad (26)$$

where we have explicitly solved the last equation for ω_t . We used that $\gamma[\omega_t] = \gamma$ and $T[\omega_t] = T_c$ throughout the work stroke and W_0 denotes the upper branch of the Lambert W function, which is defined as the solution to

$$x \equiv W[x]e^{W[x]} \quad \text{for } x \geq -1/e. \quad (27)$$

Upon eliminating ω_t , the canonical equations (26) reduce to an autonomous system of first-order differential equations,

$$\begin{pmatrix} \dot{R}_t \\ \dot{\lambda}_t \end{pmatrix} = \begin{pmatrix} \Phi_R[R_t, \lambda_t] \\ \Phi_\lambda[R_t, \lambda_t] \end{pmatrix} \equiv \Phi[R_t, \lambda_t]. \quad (28)$$

The flow of the Hamiltonian vector field $\Phi[R, \lambda]$ is plotted in Fig. 4(a). As a key observation, we find that the sign of $\dot{R}_t = \Phi_R[R_t, \lambda_t]$, which determines the direction of the instantaneous heat flux $J_t = \hbar\omega_t \dot{R}_t/2$, does not change along the optimal trajectories. Hence, since our aim is to maximize

the heat extraction from the cold reservoir, the initial values R_0 and λ_0 have to be chosen such that

$$\dot{R}_0 = \Phi_R[R_0, \lambda_0] > 0. \quad (29)$$

Solving (28) under this condition and inserting the result into the third canonical equations (26) yields the protocol

$$\omega_t^p = \frac{T_c}{\hbar} \ln \left[\frac{2 - 2C_1 W_{-1}[C_2 e^{-\gamma t}] - 1}{C_1 W_{-1}[C_2 e^{-\gamma t}]^2} \right] \quad (30)$$

and the corresponding state trajectory

$$R_t^p = C_1(1 + W_{-1}[C_2 e^{-\gamma t}])^2 - C_1 - 1. \quad (31)$$

Here W_{-1} denotes the lower branch of the Lambert W function and the constants C_1 and C_2 can be expressed in terms of the initial values R_0 and ω_0 , see Appendix A. We note that the results (30) and (31) can also be obtained using a brute-force approach, where the dynamical constraint (20) is solved explicitly rather than being enforced through a Lagrange multiplier. (For further details see Appendix A.) However, this approach crucially relies on the one-to-one correspondence (20) between the derivative \dot{R}_t of the state variable and the control parameter ω_t . It is therefore not generally applicable.

To close the optimal cycle, the reset stroke has to restore the initial state R_0 of the system in minimal time. According to Pontryagin's principle, the corresponding protocol can be found by minimizing the effective Hamiltonian

$$H_r[R_t, \lambda_t, \omega_t] = 1 + \lambda_t F[R_t, \omega_t], \quad (32)$$

with respect to ω_t . The variables R_t and λ_t thereby have to obey the canonical equations

$$\dot{R}_t = F[R_t, \omega_t] \quad \text{and} \quad \dot{\lambda}_t = \Gamma^+[\omega_t] \lambda_t \quad (33)$$

and the additional constraint

$$H_r[R_{\tau'}, \lambda_{\tau'}, \omega_{\tau'}] = 0 \quad (34)$$

at the yet undetermined optimal switching time τ' .

This problem can be approached as follows. First, we observe that (34) implies

$$\lambda_{\tau'} = -1/F[R_{\tau'}, \omega_{\tau'}] = -1/\dot{R}_{\tau'}. \quad (35)$$

Since R_t increases monotonically during the work stroke, it has to decrease during the reset. Consequently, we have to choose $\lambda_{\tau'} > 0$. Minimizing the effective Hamiltonian (32) at the switching time τ' is then equivalent to minimizing $F[R_{\tau'}, \omega_{\tau'}]$. Second, the generator F is a monotonically decreasing function of $\omega_{\tau'}$ for any admissible value of $R_{\tau'}$. Thus, it follows that $\omega_{\tau'} = \omega_{\max}$, i.e., the control parameter abruptly jumps to its maximum at the beginning of the reset stroke. Third, owing to (33), the sign of the Lagrange multiplier is conserved along its optimal trajectory. Therefore, the same argument applies at any later time $t > \tau'$ and we can conclude that $\omega_t^p = \omega_{\max}$ throughout the reset stroke. We note that this result could have been inferred directly from the Bloch equation (20) and the observation $\partial_{\omega_t} F[R_t, \omega_t] < 0$, which entails that the reset can always be accelerated by increasing ω_t . However, here we have chosen to follow the formal scheme of Sec. II to illustrate the use of Pontryagin's principle.

Finally, we have to make sure that the state R_t is continuous throughout the cycle. To this end, its trajectory during the reset stroke,

$$R_t^p = R_0 e^{\Gamma^+(\tau-t)} + (\Gamma^-/\Gamma^+)(e^{\Gamma^+(\tau-t)} - 1), \quad (36)$$

with $\Gamma^{\pm} \equiv \Gamma^{\pm}[\omega_{\max}]$, has to match the optimal work-stroke trajectory (31) at τ' , see Fig. 4(b). Numerically solving this condition yields the switching time τ' and completes the optimal protocol $\omega_t^p[R_0, \omega_0]$ [67]. Inserting this protocol back into the functional (23) together with (31) and (36) gives the maximal heat extraction $Q_c[R_0, \omega_0]$.

This function must now be maximized over the admissible range of initial values R_0 and ω_0 , which is restricted by the conditions

$$\begin{aligned} R_0 &< -\tanh[\hbar\omega_0/(2T_c)], \\ R_0 &> -\tanh[\hbar\omega_{\max}/(2T_h)], \end{aligned} \quad (37)$$

and the requirement that $\omega_0 \leq \omega'$, see Fig. 4(c). The constraints (37) follow from (29) and (36), respectively. They ensure that the heat extraction $Q_c[R_0, \omega_0]$ is positive and that the initial state of the system can be restored during the reset. To determine the maximal extracted heat Q_c^{\max} and the corresponding initial values, we employ a constrained optimization algorithm [68], which finds Q_c^{\max} either inside the admissible range (37) or on the boundary $\omega_0 = \omega'$.

Figure 5(a) summarizes the results of this section. The first plot shows the optimal cooling power Q_c^{\max}/τ as a function of the cycle time τ for different values of the high temperature T_h . We find that Q_c^{\max}/τ generally decreases with τ . Hence, for a large cooling power, the device must be operated fast. For similar recent findings, the reader may consult Refs. [28,48]. Furthermore, the cooling power becomes successively smaller as T_h increases. This result confirms the natural expectation that the microcooler becomes less effective when it has to work against a larger temperature gradient.

Figure 5(b) illustrates the general behavior of our model during the optimal cycle. In the work stroke, the state variable R_t^p monotonically increases, while the control parameter ω_t^p

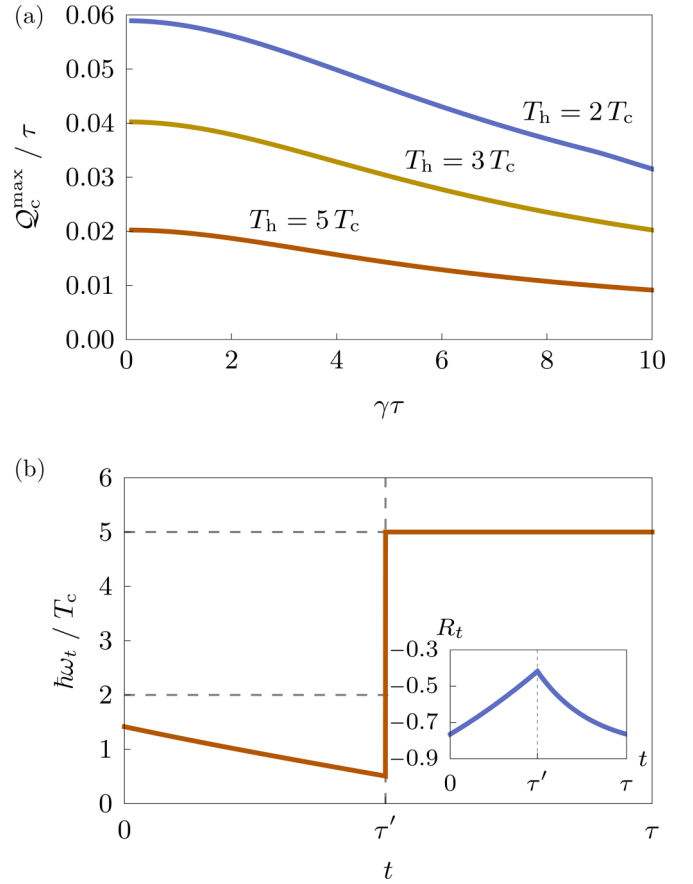


FIG. 5. Microcooler at optimal cooling power. (a) Maximum cooling power in units of γT_c as a function of the dimensionless cycle time $\gamma\tau$ for different temperatures of the hot reservoir T_h . (b) Optimal control protocol for $T_h = 2T_c$ and $\tau = 2\gamma^{-1}$. The inset shows the corresponding trajectory of the state variable R_t . Here we have used $\omega' = 2T_c/\hbar$ and $\omega_{\max} = 5T_c/\hbar$.

monotonically decreases until the switching time is reached; at this point, no more heat can be extracted from the cold reservoir in a cyclic mode of operation, i.e., the work stroke has reached the maximal length. In the reset stroke, the control parameter is constantly at its maximum, while R_t returns to its initial value following an exponential decay.

D. Maximum efficiency

Having maximized the extracted heat of our microcooler model, we now focus on its thermodynamic efficiency (12). The optimal protocol $\omega_t^\eta[Q_c^*]$, which maximizes this figure of merit for a fixed heat extraction Q_c^* , can be found using the scheme developed in Sec. II C. During the work stroke we have $\omega_t^\eta[R_0, \omega_0] = \omega_t^p[R_0, \omega_0]$, that is, for $0 \leq t \leq \tau'$ and fixed initial values R_0 and ω_0 , the protocol $\omega_t^\eta[Q_c^*]$ is given by (30). The switching time τ' can thus be determined from the constraint

$$\int_0^{\tau'} \frac{\hbar\omega_t}{2} F[R_t, \omega_t] dt = Q_c^* \quad (38)$$

using (30) and (31).

The optimal reset stroke has to restore the initial state of the system while at the same time minimizing the dissipated heat $\mathcal{Q}_h[\omega_t]$. To this end, the control protocol has to be chosen such that the effective Hamiltonian

$$H_t[R_t, \lambda_t, \omega_t] = (\omega_t + \lambda_t)(\Gamma^+[\omega_t]R_t + \Gamma^-[\omega_t]) \quad (39)$$

becomes minimal at every time $\tau' \leq t \leq \tau$, while λ_t and R_t obey the corresponding canonical equations. For a given initial value λ_0 of the Lagrange multiplier, this problem can be solved using the procedure described in Sec. II C. However, the situation is in practice complicated by the fact that λ_0 is determined only implicitly by the end-point condition $R_\tau = R_0$. It would still be possible to carry out the iteration scheme for every admissible value λ_0 and then pick the optimal protocol that closes the cycle. This approach can, however, be expected to be numerically costly and hard to implement with sufficient accuracy.

In the following we describe a more practical way of finding the optimal reset protocol. To this end, we first note that the Hamiltonian (39) is, up to its sign, identical with (25). Thus, if H_t admits a local minimum with respect to ω_t in the range $[\omega', \omega_{\max}]$, the canonical equations can be solved exactly and the reset protocol reads

$$\omega_t = \frac{T_c}{\hbar} \ln \left[\frac{2 - 2C_1 W_0 [C_2 e^{-\gamma t'}]}{C_1 W_0 [C_2 e^{-\gamma t}]^2} - 1 \right], \quad (40)$$

where C_1 and C_2 are constants. Note that, in contrast to (30), this solution must involve the upper rather than the lower branch of the Lambert W function to ensure that the state variable decreases during the reset, i.e., $\dot{R}_t = F[R_t, \omega_t] < 0$. According to Pontryagin's principle, the protocol ω_t^η either follows the monotonically increasing trajectory (40) or takes on one of the boundary values ω' or ω_{\max} . Consequently, if we assume that the optimal protocol does not jump within the reset stroke, it must have the general form shown in Fig. 6(b). Specifically, ω_t^η must be constant at ω' until a certain time τ_1 , then follow (40) until it reaches ω_{\max} , and finally remain constant until the end of the stroke. Since each protocol of this type is uniquely determined by the departure time τ_1 , this procedure induces a one-to-one mapping between τ_1 and the state of the system at the end of the reset stroke, $R_\tau = R_\tau[\tau_1]$. This map can be determined analytically from the corresponding Bloch equation. The only numerical operation that is required to determine the optimal reset protocol thus consists of solving the condition $R_\tau[\tau_1] = R_0$ for τ_1 [69].

The method described above makes it possible to find the protocol $\omega_t^\eta[R_0, \omega_0, \mathcal{Q}_c^*]$ that maximizes the efficiency of the cooling cycle for given R_0 , ω_0 , and \mathcal{Q}_c^* . Inserting this protocol into (12) and optimizing the resulting function $\eta[R_0, \omega_0, \mathcal{Q}_c^*]$ with respect to the initial values R_0 and ω_0 finally yields the maximal efficiency at given cooling power.

This figure of merit is plotted in Fig. 6 together with the corresponding optimal protocol; it approaches the Carnot limit (13) for $\mathcal{Q}_c^* \rightarrow 0$ and monotonically decays as \mathcal{Q}_c^* becomes larger. Thus, increasing the heat extraction of the microcooler inevitably reduces its maximal efficiency. This result aligns well with recent discoveries of universal trade-off relations between the extracted heat and the efficiency of mesoscopic thermal devices [39,40,44,70–73]. Furthermore, Fig. 6(a) shows that not only the maximal cooling power

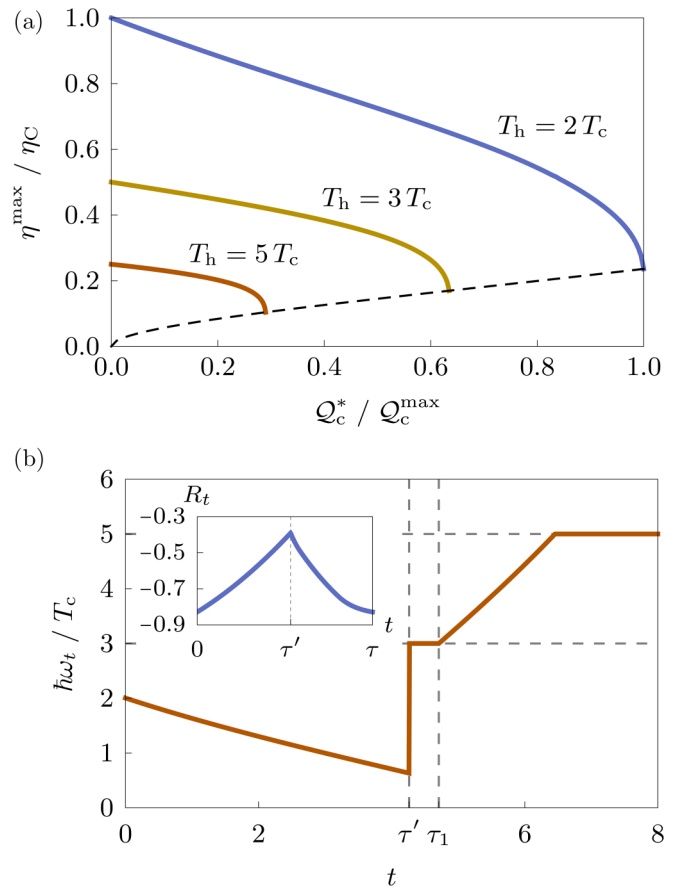


FIG. 6. Microcooler at optimal efficiency. (a) Maximum efficiency as a function of the given heat extraction \mathcal{Q}_c^* . The horizontal axis has been rescaled with the maximum heat extraction for $T_h = 2 T_c$, \mathcal{Q}_c^{\max} , and the vertical axis with the Carnot efficiency η_C for the same temperatures. The dashed line shows how the efficiency at maximal cooling power decays as the temperature gradient becomes larger. (b) Optimal control protocol leading to maximal efficiency for fixed heat extraction $\mathcal{Q}_c^* = 0.9 \mathcal{Q}_c^{\max}$. The inset shows the corresponding trajectory of the state variable R_t . Throughout this figure, we have set $\omega' = 3 T_c / \hbar$, $\omega_{\max} = 5 T_c / \hbar$, $T_h = 2 T_c$, and $\tau = 8 \gamma^{-1}$. For these parameter values, the maximum extracted heat at $T_h = 2 T_c$ is $\mathcal{Q}_c^{\max} \approx 0.297 T_c$.

but also the overall efficiency decays as the temperature of the hot reservoir becomes larger. Hence, increasing the temperature bias is generally detrimental to the performance of the microcooler.

IV. APPROXIMATION METHODS

A. Rationale

Our two-stroke scheme makes it possible to systematically optimize realistic models for mesoscopic thermal machines, as we have shown in the previous section for a superconducting microcooler. To explore the optimal performance of even more complex devices, it is often helpful to first focus on limiting regimes, where dynamical approximation methods can be used to simplify computational tasks. In this section we develop such schemes for the key limits of slow or fast driving. We thereby further extend our general framework and

prepare the stage to investigate the thermodynamic performance of mesoscopic refrigerators in the coherent regime.

B. Adiabatic response

We consider a slowly operated two-stroke refrigerator by assuming $\tau, \tau' \gg 1/\gamma$, where γ is the typical relaxation rate of the working system. Except for short transient periods at the beginning of each stroke, the system then follows the instantaneous equilibrium state $\mathbf{R}_{\text{eq}}[\omega_t]$, which is defined by the condition

$$F[\mathbf{R}_{\text{eq}}[\omega_t], \omega_t] \equiv 0. \quad (41)$$

In particular, we have

$$\mathbf{R}_{\tau'} \simeq \mathbf{R}_{\text{eq}}[\omega_w] \quad \text{and} \quad \mathbf{R}_\tau \simeq \mathbf{R}_{\text{eq}}[\omega_r], \quad (42)$$

where ω_w and ω_r are the values of the control parameter at the end of the work and the reset stroke, respectively. We note that this approximation can be systematically refined by including finite-time corrections. To this end, the time-evolution equation (1) has to be solved perturbatively by expanding the state vector \mathbf{R}_t in powers of the adiabaticity parameter $\varepsilon \equiv 1/(\gamma\tau)$ [74]. However, to keep our analysis as transparent and simple as possible, we here neglect contributions of order ε . The relations (42) significantly reduce the interdependence of work and reset stroke, and thus simplify our optimization scheme as follows.

To maximize the heat extraction (2), the work protocol has to be found by solving the canonical equations (7) for fixed initial conditions \mathbf{R}_0 and λ_0 . Since \mathbf{R}_t does not change during the quenches of ω_t , we now have $\mathbf{R}_0 = \mathbf{R}_{\text{eq}}[\omega_r]$, i.e., the initial state of the system is determined by one parameter ω_r . Moreover, to restore this state after the work stroke, it suffices to set $\omega_t = \omega_r$ for a short time $\mathcal{T}_r \simeq 1/\gamma \equiv \varepsilon\tau$. Hence, in the zeroth order with respect to ε , we have $\tau \simeq \tau'$ and the reset stroke does not have to be optimized separately. In fact, the optimal protocol ω_t^p is obtained by extending the work stroke over the entire cycle time τ and maximizing the resulting heat extraction over $N + 1$ parameters given by λ_0 and ω_r .

Our second optimization criterion requires us to minimize the dissipated heat (3) for given cooling power Q_c^*/τ . To this end, both strokes have to be taken into account. Specifically, after finding the optimal work protocol $\omega_t[\omega_r, \lambda_0]$ as before, we first have to determine the switching time $\tau'[\omega_r, \lambda_0, Q_c^*]$ such that $Q_c[\omega_t] = Q_c^*$, cf. (15). To find the optimal reset protocol, the objective functional (16) has to be minimized using fixed initial conditions $\mathbf{R}_{\tau'} = \mathbf{R}_{\text{eq}}[\omega_w]$ and $\lambda_{\tau'}$ for the state variables and Lagrange multipliers, respectively. Here ω_w is determined by ω_r and λ_0 ; $\lambda_{\tau'}$ has to be chosen such that the cycle condition $\omega_\tau = \omega_r$ is satisfied. Owing to this constraint, the optimal protocol $\omega_t^\eta[\omega_r, \lambda_0, \lambda_{\tau'}, Q_c^*]$ effectively depends on $2N$ free parameters, which have to be eliminated by minimizing the corresponding heat release $Q_h[\omega_r, \lambda_0, \lambda_{\tau'}]$. Though generally nontrivial, this procedure is still significantly simpler than the full optimization, which involves N boundary conditions to ensure that $\mathbf{R}_\tau = \mathbf{R}_0$. By contrast, here only one constraint has to be respected. The continuity of the state \mathbf{R}_t is then enforced by the adiabaticity condition (42).

C. High-frequency response

Having understood how to optimize a two-stroke refrigerator in adiabatic response, we now consider the opposite limit $\tau, \tau' \ll 1/\gamma$. In this regime, the state vector \mathbf{R}_t changes only slightly during the individual strokes, since the working system is unable to follow the rapid variations of the control parameter ω_t . Therefore, we can use the approximations

$$\begin{aligned} \mathbf{R}_t &\simeq \mathbf{R}_0 + t\dot{\mathbf{R}}_0 = \mathbf{R}_0 + tF[\mathbf{R}_0, \omega_0] \quad \text{and} \\ \mathbf{R}_t &\simeq \mathbf{R}_{\tau'} + (t - \tau')\dot{\mathbf{R}}_{\tau'} = \mathbf{R}_{\tau'} + (t - \tau')F[\mathbf{R}_{\tau'}, \omega_{\tau'}] \end{aligned} \quad (43)$$

to describe the work and the reset stroke, respectively. The initial states \mathbf{R}_0 and $\mathbf{R}_{\tau'}$ are thereby fully determined as functions of ω_0 and $\omega_{\tau'}$ by the requirement that \mathbf{R}_t is continuous throughout the cycle. Thus, inserting the expansions (43) into (2) and (3) and neglecting second-order corrections in $1/\varepsilon \equiv \gamma\tau$ yields

$$\begin{aligned} Q_c[\omega_t] &\simeq \tau'J[\mathbf{R}_0, \omega_0] \equiv Q_c[\tau', \omega_0, \omega_{\tau'}] \quad \text{and} \\ Q_h[\omega_t] &\simeq (\tau' - \tau)J[\mathbf{R}_{\tau'}, \omega_{\tau'}] \equiv Q_h[\tau', \omega_0, \omega_{\tau'}]. \end{aligned} \quad (44)$$

These expressions show that both the extracted and the released heat of the device now depend only on the switching time τ' and the initial values of the work and the reset protocols ω_0 and $\omega_{\tau'}$. Consequently, any control protocol ω_t can be mimicked with a step profile

$$\omega_t^{\text{HF}}[\tau', \omega_0, \omega_{\tau'}] = \omega_0 + (\omega_{\tau'} - \omega_0)\Theta[t - \tau'], \quad (45)$$

where Θ denotes the Heaviside function. In particular, the optimal protocols ω_t^p and $\omega_t^\eta[Q_c^*]$ adopt the form (45) in the fast-driving limit. For ω_t^p , the free parameters τ', ω_0 , and $\omega_{\tau'}$ must be determined by maximizing $Q_c[\tau', \omega_0, \omega_{\tau'}]$. Analogously, $\omega_t^\eta[Q_c^*]$ is found by minimizing $Q_h[\tau', \omega_0, \omega_{\tau'}]$ under the constraint $Q_c[\tau', \omega_0, \omega_{\tau'}] = Q_c^*$.

The high-frequency approximation provides a simple yet powerful tool to explore the performance limits of mesoscopic refrigerators. In fact, due to the universal form (45) of the high-frequency protocol, our general scheme can be reduced to relatively simple three-parameter optimizations. Moreover, the approximations (43) and (44) can be systematically refined by including higher-order corrections in $1/\varepsilon$, and thus introducing more and more variational parameters given by the higher derivatives of ω_t at $t = 0$ and $t = \tau'$.

D. Semiclassical microcooler revisited

Before moving on to the full quantum regime, we now illustrate our approximation scheme for the semiclassical microcooler. For the sake of brevity, we here focus on maximum cooling power as our optimization criterion.

In the adiabatic limit, the reset stroke does not have to be considered explicitly and the optimal protocol ω_t^p is given by (30) for $0 \leq t \leq \tau$. The two constants C_1 and C_2 thereby have to be chosen such that the extracted heat $Q_c[\omega_t] = Q_c[C_1, C_2]$ becomes maximal. This condition is equivalent to optimizing the reset level $\omega_r \in [\omega', \omega_{\text{max}}]$ of the control parameter and the initial value λ_0 of the Lagrange multiplier, as described in the first part of Sec. IV B.

The resulting optimal cooling power is shown in Fig. 7 as a function of the dimensionless cycle time $\gamma\tau$, which corresponds to the inverse adiabaticity parameter $1/\varepsilon$. This

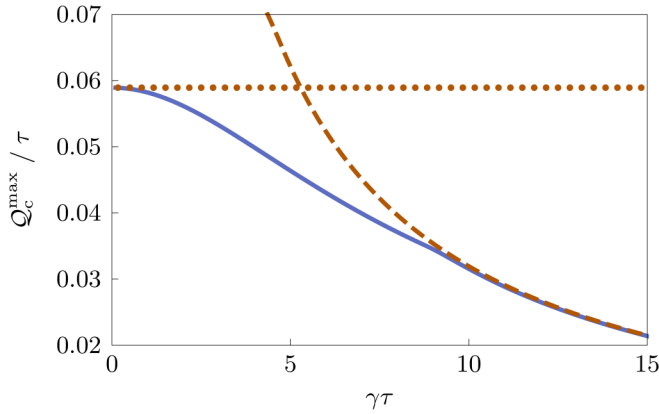


FIG. 7. Quantum microcooler at slow and fast driving. The plot shows the maximum cooling power Q_c^{\max}/τ in units of γT_c as a function of the inverse adiabaticity parameter $1/\varepsilon = \gamma\tau$. In the limits $\gamma\tau \gg 1$ and $\gamma\tau \ll 1$, the exact result from Sec. III C (solid line) approaches the adiabatic (dashed line) and high-frequency (dotted line) approximations, respectively. The parameters in this figure are the same as in Fig. 5(a), i.e., the blue curves in both plots are identical.

plot confirms that our adiabatic response scheme is indeed accurate for $\varepsilon \ll 1$. In fact, the adiabatic approximation for Q_c^{\max}/τ departs from the exact result obtained in Sec. III C only at $1/\varepsilon \equiv \gamma\tau \simeq 10$.

In the fast driving regime, the cooling power is maximized by a step protocol with the general form (45). The variational parameters ω_0 , $\omega_{\tau'}$, and τ' can be determined exactly by maximizing the heat extraction (23) after inserting (43) and (45) and neglecting second-order corrections in $1/\varepsilon = \gamma\tau$. We find that the optimal switching time is given by

$$\tau^*[\omega_0, \omega_{\tau'}] \equiv \frac{\sqrt{\Gamma_0^+ \Gamma_{\tau'}^+ - \Gamma_{\tau'}^+}}{\Gamma_0^+ - \Gamma_{\tau'}^+} \tau \quad (46)$$

as a function of the levels ω_0 and $\omega_{\tau'}$ of the protocol ω_t^{HF} . Here we have used the abbreviation $\Gamma_t^+ \equiv \Gamma^+[\omega_t]$. The optimal reset level is $\omega_{\tau'}^* = \omega_{\max}$ and the optimal work level follows from maximizing the cooling power

$$Q_c^{\max}/\tau = \max_{\omega_0} \{ \hbar\omega_0\gamma(1 - 2\tau^*[\omega_0, \omega_{\tau'}^*]/\tau) \}. \quad (47)$$

Note that this expression is independent of ε , since here we consider only the lowest order of the high-frequency expansion. Still, as shown in Fig. 7, the exact optimal cooling power approaches the constant value (47) for $1/\varepsilon \lesssim 1$, thus confirming the validity of our approximation scheme for the fast-driving regime.

V. QUANTUM MICROCOOLER II: COHERENT REGIME

As a key application of our approximation methods, we will now show how the cooling power of the microcooler illustrated in Fig. 3 can be optimized in the full quantum regime. To this end, we first recall the qubit Hamiltonian (18),

$$H_t \equiv \frac{\hbar\Delta}{2}\sigma_x + \frac{\hbar\omega_t}{2}\sigma_z, \quad (48)$$

which describes the working system of this device. If the tunneling energy Δ is not negligible, the periodic state that emerges due to cyclic variation of the control parameter ω_t features coherences between the two energy levels of the qubit. The corresponding density matrix must therefore be parametrized in the general form

$$\rho_t \equiv \frac{1}{2}(\mathbb{1} + \mathbf{R}_t \cdot \boldsymbol{\sigma}), \quad (49)$$

where $\boldsymbol{\sigma} \equiv (\sigma_x, \sigma_y, \sigma_z)^T$ is the vector of Pauli matrices and the state vector \mathbf{R}_t fulfills the Bloch equation [18,45]

$$\begin{aligned} \dot{\mathbf{R}}_t &= \mathbf{F}[\mathbf{R}_t, \Omega_t] \\ &\equiv \begin{bmatrix} -\Gamma_t^+ \frac{\Omega_t^2 + \Delta^2}{2\Omega_t^2} & -\omega_t & -\Gamma_t^+ \frac{\omega_t \Delta}{2\Omega_t^2} \\ \omega_t & -\frac{1}{2}\Gamma_t^+ & -\Delta \\ -\Gamma_t^+ \frac{\omega_t \Delta}{2\Omega_t^2} & \Delta & -\Gamma_t^+ \frac{2\Omega_t^2 - \Delta^2}{2\Omega_t^2} \end{bmatrix} \mathbf{R}_t - \frac{\Gamma_t^-}{\Omega_t} \begin{bmatrix} \Delta \\ 0 \\ \omega_t \end{bmatrix}. \end{aligned} \quad (50)$$

Here the rates $\Gamma_t^\pm \equiv \Gamma^\pm[\Omega_t]$ are defined as in (20) with ω_t replaced by the instantaneous level splitting

$$\Omega_t \equiv \sqrt{\Delta^2 + \omega_t^2}, \quad (51)$$

which we will treat as the effective control parameter of the system from here onwards.

In order to extend our step-rate model to the coherent regime, we have to take into account that Ω_t cannot vanish for finite Δ . Therefore, the lower bound 0 in the coupling factor (22) has to be replaced with $\Omega_{\min} = \Delta$. Furthermore, also the threshold frequency Ω' , which now takes the role of ω' in the switching condition (21) for the reservoir temperature, has to be larger than Δ .

Upon inserting (48) and (49) into the weak-coupling expression (4) for the instantaneous heat flux, the mean heat extraction in the coherent regime becomes a functional of Ω_t ,

$$\begin{aligned} Q_c[\Omega_t] &\equiv \int_0^{\tau'} J[\mathbf{R}_t, \Omega_t] dt \\ &\equiv - \int_0^{\tau'} \left(\frac{\hbar\Gamma_t^+}{2} (\Delta R_t^x + \omega_t R_t^z) + \frac{\hbar\Gamma_t^-}{2} \Omega_t \right) dt, \end{aligned} \quad (52)$$

which could, in principle, be optimized by applying the three-step procedure of Sec. II B. This endeavor can be expected to be technically quite involved, since the periodicity constraint $\mathbf{R}_\tau = \mathbf{R}_0$ now leads to three independent boundary conditions for the reset stroke, while only a single parameter is available to control the time evolution of the state \mathbf{R}_t . However, to understand how the optimal performance of the microcooler changes in the quantum regime, it is sufficient to determine the impact of the tunneling energy Δ on its maximum cooling power. For this purpose, it is not necessary to carry out the full optimization procedure. Instead, we can focus our analysis on the limits of slow and fast driving, where our approximation schemes enable a simple and physically transparent approach.

In the adiabatic-response regime, only the work stroke needs to be optimized [75]. To this end, we first integrate the canonical equations corresponding to the effective Hamiltonian

$$H_w[\mathbf{R}_t, \lambda_t, \Omega_t] = J[\mathbf{R}_t, \Omega_t] + \lambda_t \cdot \mathbf{F}[\mathbf{R}_t, \Omega_t] \quad (53)$$

for the given initial conditions

$$\mathbf{R}_0 = \mathbf{R}_{\text{eq}}[\Omega_r] = -\frac{\Gamma^-[\Omega_r]}{\Gamma^+[\Omega_r]} \left(\frac{\Delta}{\Omega_r}, 0, \frac{\sqrt{\Omega_r^2 - \Delta^2}}{\Omega_r} \right)^\top \quad (54)$$

and λ_0 , see Appendix B. The parameters Ω_r and λ_0 then have to be determined by maximizing the heat extraction $\mathcal{Q}_c[\Omega_r] = \mathcal{Q}_c[\Omega_r, \lambda_0]$. This task is *a priori* challenging, since the initial Lagrange multipliers λ_0^x and λ_0^y are left unbounded by physical constraints. To overcome this problem, we use an iterative algorithm, which tracks the maximum of $\mathcal{Q}_c[\Omega_r, \lambda_0]$ as Δ is increased in small steps starting from its semiclassical value $\Delta = 0$. This approach relies on the implicit assumption that the global maximum of the function $\mathcal{Q}_c[\Omega_r, \lambda_0]$ follows a continuous trajectory in the four-dimensional space of variational parameters, which is justified *a posteriori* by the physical consistency of our results.

In the high-frequency regime, the cooling power is maximized by the step protocol

$$\Omega_r^{\text{HF}}[\tau', \Omega_0, \Omega_{\tau'}] = \Omega_0 + (\Omega_{\tau'} - \Omega_0)\Theta[t - \tau']. \quad (55)$$

As in the semiclassical case discussed in Sec. IV D, the variational parameters τ' , Ω_0 , and $\Omega_{\tau'}$ can be determined by maximizing the corresponding cooling power in first order with respect to $1/\varepsilon = \gamma\tau$. The resulting expression for $\mathcal{Q}_c[\tau', \Omega_0, \Omega_{\tau'}]$ is rather involved and we do not show it here. The optimal variational parameters can however be determined numerically. We note in particular that this optimization yields $\Omega_{\tau'}^* = \Omega_{\text{max}}$.

Figure 8 shows the result of our analysis. In both the adiabatic and the high-frequency limit, the maximum cooling power monotonically decreases from its semiclassical value to 0 as Δ increases. This behavior can be explained as follows. The tunneling energy Δ corresponds to the minimal gap between the energy levels of the working system, see Fig. 3. Increasing this parameter reduces the amount of thermal energy that can be absorbed during the work stroke. As Δ approaches a certain critical value, the capacity of the working system to pick up heat from the cold reservoir becomes too small for the device to operate properly. The optimal protocol then keeps the system practically in equilibrium at the low temperature T_c throughout the work stroke and the cooling power becomes zero. Since this general picture can be expected to prevail also for intermediate driving speed, we can conclude that to engineer a powerful microcooler, the tunneling energy of the qubit must be kept as small as possible.

VI. DISCUSSION AND OUTLOOK

Our work provides a systematic scheme to optimize periodic driving protocols for mesoscopic two-stroke machines. Though developed here specifically for refrigerators, this general framework can easily be adapted to other types of thermal devices. Reciprocating heat engines, for example, use a periodically driven working system to convert thermal energy into mechanical power [31,59,76,77]. Within our two-stroke approach, this process can be described as a reversed cooling cycle. That is, the system picks up heat from a hot reservoir in the first stroke and returns to its initial state while being in contact with a cold reservoir in the second stroke. To achieve optimal performance, the engine has to generate

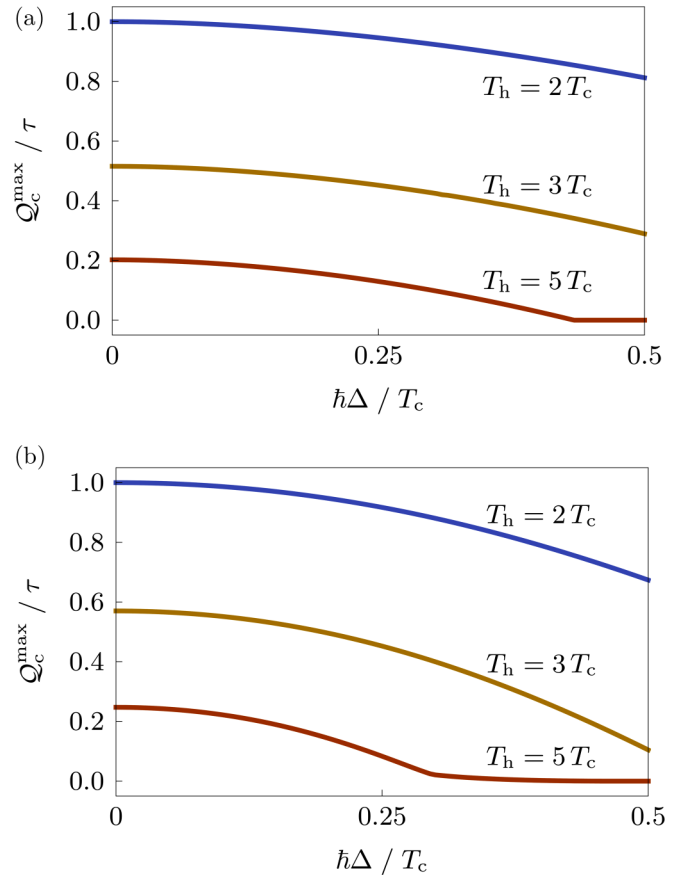


FIG. 8. Optimal cooling power of the coherent microcooler as a function of the tunneling energy Δ . (a) Maximum cooling power in the adiabatic regime ($\gamma\tau = 10$) for different temperatures of the hot reservoir. (b) Maximum cooling power in the high-frequency regime (independent of $\gamma\tau$). Here we have used $\Omega' = 1.5 T_c/\hbar$, $\Omega_{\text{max}} = 3 T_c/\hbar$, and $\hbar\gamma = T_c$. For comparison with the semiclassical model, the cooling power has been normalized with its value at $\Delta = 0$ and $T_h = 2 T_c$ in both plots.

as much work output as possible from a given amount of thermal input energy. Owing to the first law, this optimization criterion is equivalent to minimizing the dissipated heat during the reset while keeping the heat uptake during the work stroke fixed. The corresponding optimal control protocol can thus be determined using the three-step procedure of Sec. II C.

The performance figures of mesoscopic thermal devices, such as power and efficiency, can generally not be optimized simultaneously. Instead, they are subject to universal trade-off relations as several recent studies have shown [30,71,72,78,79]. As one of its potential key applications, our two-stroke scheme makes it possible to test the quality of these constraints under practical conditions. Furthermore, covering both classical and quantum systems, the framework developed in this article might open a new avenue to systematically explore the impact of coherence on the performance of thermodynamic cycles, a central topic in quantum thermodynamics, see for example Refs. [25,59,78,80–85].

To facilitate future investigations in these directions, our scheme can be combined with a variety of dynamical approximation methods. In Sec. IV, for example, we have shown how

adiabatic and high-frequency expansion techniques can be included. To this end, we have solved the dynamical constraint perturbatively assuming that the external driving is either slow or fast compared to the relaxation time of the working system. This approach makes it possible to circumvent the use of Lagrange multipliers and thus reduces the amount of dynamical parameters in the optimization problem. An alternative strategy could use the variational equations in the extended parameter space as a starting point. Specifically, the canonical structure of these equations makes it possible to implement a variety of tools that were originally developed for the description of classical Hamiltonian systems including adiabatic gauge potentials [86], shortcuts to adiabaticity [87,88], or nonlinear generalizations of the Magnus expansion [89].

Integrating such advanced methods into our general framework will inevitably require a reliable reference to assess their practicality and accuracy. Such a testbed is provided in Sec. III, where we have developed a simple and physically transparent model of a quantum microcooler, whose optimal operation cycle can be determined exactly. In fact, this case study provides both a demonstration that our theoretical framework is directly applicable to ongoing experiments with engineered quantum systems and a valuable benchmark for further advances in theoretical optimization methods.

ACKNOWLEDGMENTS

We thank J. P. Pekola for useful discussions. K.B. acknowledges support from the Academy of Finland (Contract No. 296073). This work was supported by the Academy of Finland (Projects No. 308515 and No. 312299). All authors are associated with the Centre for Quantum Engineering at Aalto University.

APPENDIX A: ALTERNATIVE OPTIMIZATION SCHEME FOR THE SEMICLASSICAL MICROCOOLER

In Sec. III C we have derived the optimal work protocol (40) for the semiclassical microcooler by enforcing the dynamical constraint (20) with a Lagrange multiplier. Here we present an alternative method to obtain the result (40), which exploits the one-to-one correspondence between the control parameter and the derivative of the state variable in this model.

We proceed as follows. First, solving Eq. (20) for ω_t yields

$$\omega_t = \frac{T_c}{\hbar} \ln \left[\frac{\gamma(1 - R_t)}{\dot{R}_t + \gamma(1 + R_t)} \right]. \quad (\text{A1})$$

Upon inserting this expression into (23), the objective functional becomes

$$\mathcal{Q}_c[R_t] = \int_0^{\tau'} J[R_t, \dot{R}_t] dt, \quad (\text{A2})$$

where the effective Lagrangian

$$J[R_t, \dot{R}_t] \equiv \frac{T_c}{2} \dot{R}_t \ln \left[\frac{\gamma(1 - R_t)}{\dot{R}_t + \gamma(1 + R_t)} \right] \quad (\text{A3})$$

does not explicitly depend on time. Consequently, the corresponding effective Hamiltonian is a constant of motion

given by

$$4\gamma C_1 \equiv \frac{\dot{R}_t^2}{\dot{R}_t + \gamma(1 + R_t)}. \quad (\text{A4})$$

Using (20), C_1 can be expressed in terms of the initial values R_0 and ω_0 as

$$C_1 = \frac{1}{1 - R_0} \left(R_0 \cosh \left[\frac{\hbar\omega_0}{2T_c} \right] + \sinh \left[\frac{\hbar\omega_0}{2T_c} \right] \right)^2. \quad (\text{A5})$$

This expression shows that C_1 is non-negative. Furthermore, for $C_1 = 0$, (A4) and (A5) imply $R_t = R_0 = -\tanh[\hbar\omega_0/(2T_c)]$ and $\omega_t = \omega_0$, that is, the system is in equilibrium throughout the cycle and the average heat extraction (A2) becomes zero.

Second, solving (A4) for \dot{R}_t gives

$$\dot{R}_t = 2\gamma [C_1 \pm \sqrt{C_1(C_1 + 1 + R_t)}], \quad (\text{A6})$$

where only the positive branch of the square root leads to $\dot{R}_t > 0$ and thus positive heat extraction. Since we require that the control parameter ω_t , which is given by (A1) in terms of R_t , does not jump during the work stroke, both R_t and \dot{R}_t must be continuous. We can thus neglect the negative branch in (A6). Note that this choice implies the constraint $\dot{R}_0 = F[R_0, \omega_0] > 0$ on the initial values R_0 and ω_0 , cf. (29) and (37).

Third, solving the differential equation (A6) under this condition yields

$$R_t^p = -1 + C_1 \{ (1 + W_{-1}[C_2 e^{-\gamma t}])^2 - 1 \}, \quad (\text{A7})$$

where the dimensionless constant C_2 is given by

$$C_2 = W^{-1} \left[\frac{2(1 - R_0)}{(1 + R_0) e^{\hbar\omega_0/(kT_c)} - (1 - R_0)} \right], \quad (\text{A8})$$

with $W^{-1}[x] \equiv x e^x$. Thus, we have recovered the result (31) of the main text.

APPENDIX B: OPTIMAL WORK STROKE OF THE COHERENT MICROCOOLER

The optimal work stroke of the coherent microcooler discussed in Sec. V is described by the effective Hamiltonian

$$H_w[\mathbf{R}_t, \boldsymbol{\lambda}_t, \Omega_t] = \frac{T_c}{2} \boldsymbol{\lambda}_t \cdot \mathbf{F}[\mathbf{R}_t, \Omega_t] - \frac{\hbar\Gamma_t^+}{2} (\Delta R_t^x + \omega_t R_t^z) - \frac{\hbar\Gamma_t^-}{2} \Omega_t, \quad (\text{B1})$$

where we rescaled the Lagrange multipliers λ_t by a factor of $T_c/2$ compared with (53) for convenience. The corresponding canonical equations for the state variables and Lagrange

multipliers are given by

$$\dot{\mathbf{R}}_t = \mathbf{F}[\mathbf{R}_t, \Omega_t]$$

$$\equiv \begin{bmatrix} -\Gamma_t^+ \frac{\Omega_t^2 + \Delta^2}{2\Omega_t^2} & -\omega_t & -\Gamma_t^+ \frac{\omega_t \Delta}{2\Omega_t^2} \\ \omega_t & -\frac{1}{2}\Gamma_t^+ & -\Delta \\ -\Gamma_t^+ \frac{\omega_t \Delta}{2\Omega_t^2} & \Delta & -\Gamma_t^+ \frac{2\Omega_t^2 - \Delta^2}{2\Omega_t^2} \end{bmatrix} \mathbf{R}_t - \frac{\Gamma_t^-}{\Omega_t} \begin{bmatrix} \Delta \\ 0 \\ \omega_t \end{bmatrix} \quad (\text{B2})$$

and

$$\dot{\boldsymbol{\lambda}}_t = \begin{bmatrix} \Gamma_t^+ \frac{\Omega_t^2 + \Delta^2}{2\Omega_t^2} & -\omega_t & \Gamma_t^+ \frac{\omega_t \Delta}{2\Omega_t^2} \\ \omega_t & \frac{1}{2}\Gamma_t^+ & -\Delta \\ \Gamma_t^+ \frac{\omega_t \Delta}{2\Omega_t^2} & \Delta & \Gamma_t^+ \frac{2\Omega_t^2 - \Delta^2}{2\Omega_t^2} \end{bmatrix} \boldsymbol{\lambda}_t + \frac{\hbar \Gamma_t^+}{T_c} \begin{bmatrix} \Delta \\ 0 \\ \omega_t \end{bmatrix}, \quad (\text{B3})$$

respectively. We recall that the energy bias ω_t and the level splitting Ω_t are related by $\omega_t = \sqrt{\Omega_t^2 - \Delta^2}$.

The evolution equations (B2) and (B3) are coupled by the algebraic constraint

$$\frac{\partial}{\partial \Omega_t} H_w[\mathbf{R}_t, \boldsymbol{\lambda}_t, \Omega_t] = 0. \quad (\text{B4})$$

This differential-algebraic system could, in principle, be integrated by solving the algebraic constraint for $\Omega_t = \Omega[\mathbf{R}_t, \boldsymbol{\lambda}_t]$. Equations (B2) and (B3) would then become an ordinary system of differential equations, which could be integrated using standard techniques. This approach has been used for the semiclassical microcooler in Sec. III C. However, owing to its complicated structure, solving the constraint (B4) for Ω_t is hard to implement in practice.

Instead, it is more convenient to transform the Bloch equations into a co-rotating frame. To this end, we define the transformed Bloch vector \mathbf{r}_t by replacing the static parametrization (49) with

$$\rho_t \equiv \frac{1}{2} V_t (1 + \mathbf{r}_t \cdot \boldsymbol{\sigma}) V_t^\dagger. \quad (\text{B5})$$

Here V_t denotes the unitary matrix

$$V_t \equiv \begin{pmatrix} \cos[\varphi_t/2] & -\sin[\varphi_t/2] \\ \sin[\varphi_t/2] & \cos[\varphi_t/2] \end{pmatrix} \quad (\text{B6})$$

with $\tan[\varphi_t] \equiv \Delta/\omega_t$, which diagonalizes the instantaneous Hamiltonian H_t . In fact, the vectors \mathbf{R}_t and \mathbf{r}_t differ by a rotation in the x - z plane by the angle φ_t . This change of coordinates separates the population and the coherence degrees of freedom of the density matrix, which are now parametrized by r_t^z and $r_t^{x,y}$, respectively. Note that, in contrast to \mathbf{R}_t , the transformed Bloch vector \mathbf{r}_t is not continuous at the jumps of the control protocol Ω_t ; if V_{t-dt} and V_t are the rotation operators corresponding to the Hamiltonian before and after the jump, respectively, the accompanying jump in \mathbf{r}_t is determined by the condition

$$r_t^k = \text{tr}[V_t^\dagger V_{t-dt} (\mathbf{r}_{t-dt} \cdot \boldsymbol{\sigma}) V_{t-dt}^\dagger V_t \sigma_k]/2. \quad (\text{B7})$$

In the following, we will show how the optimal work protocol can be calculated in the rotating frame. To this end, we first observe that the transformed Bloch equation reads

$$\dot{\mathbf{r}}_t = \begin{bmatrix} -\Gamma_t^+/2 & -\Omega_t & -\dot{\varphi}[\Omega_t, \dot{\Omega}_t] \\ \Omega_t & -\Gamma_t^+/2 & 0 \\ \dot{\varphi}[\Omega_t, \dot{\Omega}_t] & 0 & -\Gamma_t^+ \end{bmatrix} \mathbf{r}_t - \begin{bmatrix} 0 \\ 0 \\ \Gamma_t^- \end{bmatrix}. \quad (\text{B8})$$

As an artifact of the time-dependent parametrization (B5), the right-hand side of (B8) now depends on the time derivative of the control parameter $\dot{\Omega}_t$. Our general optimization scheme can, however, still be applied without major modifications since $\dot{\Omega}_t$ has no physical significance here.

The transformed vector of Lagrange multipliers $\boldsymbol{\Lambda}_t$ satisfies the evolution equation

$$\dot{\boldsymbol{\Lambda}}_t = \begin{bmatrix} \Gamma_t^+/2 & -\Omega_t & -\dot{\varphi}[\Omega_t, \dot{\Omega}_t] \\ \Omega_t & \Gamma_t^+/2 & 0 \\ \dot{\varphi}[\Omega_t, \dot{\Omega}_t] & 0 & \Gamma_t^+ \end{bmatrix} \boldsymbol{\Lambda}_t + \frac{\hbar \Omega_t}{T_c} \begin{bmatrix} 0 \\ 0 \\ \Gamma_t^+ \end{bmatrix} \quad (\text{B9})$$

in the rotating frame and the algebraic constraint (B4) becomes

$$\begin{aligned} & \frac{\hbar \Delta}{T_c} \left\{ 2\Lambda_t^x (1 - e^{-W_t}) + (2W_t r_t^x + \Lambda_t^z r_t^x + \Lambda_t^x r_t^z) (1 + e^{-W_t}) \right. \\ & \quad \left. + \frac{2T_c}{\hbar \gamma} W_t (\Lambda_t^y r_t^z - \Lambda_t^z r_t^y) \right\} \\ & = \frac{\hbar \Omega_t}{T_c} \frac{\hbar \omega_t}{T_c} \left\{ 2(1 + r_t^z) - \frac{2T_c}{\hbar \gamma} (\Lambda_t^y r_t^x - \Lambda_t^x r_t^y) \right. \\ & \quad \left. - e^{-W_t} [2(1 - r_t^z) (1 - W_t - \Lambda_t^z) + \Lambda_t^x r_t^x + \Lambda_t^y r_t^y] \right\} \end{aligned} \quad (\text{B10})$$

in the new variables, where $W_t = \hbar \Omega_t / T_c$.

In order to obtain a closed system of differential equations, we have to express $\dot{\Omega}_t$ in terms of \mathbf{r}_t , $\boldsymbol{\Lambda}_t$, and Ω_t . To this end, we take the time derivative of the algebraic constraint (B10) and then use (B8) and (B9) to eliminate $\dot{\mathbf{r}}_t$ or $\dot{\boldsymbol{\Lambda}}_t$. The resulting expression can be rewritten in the form

$$\dot{\Omega}_t = \dot{\Omega}[\mathbf{r}_t, \boldsymbol{\Lambda}_t, \Omega_t]. \quad (\text{B11})$$

The relation (B11) enables the following strategy to find the optimal time evolution. We first choose initial values $(\mathbf{r}_0, \boldsymbol{\Lambda}_0, \Omega_0)$, which are compatible with the algebraic constraint (B10). For this purpose, we note that (B10) is a linear equation in \mathbf{r}_t and $\boldsymbol{\Lambda}_t$. Therefore, it is straightforward to determine, for example, Λ_0^z if all other initial values are given. Equations (B8), (B9), and (B11) then form an autonomous system of seven first-order differential equations, which can be treated as a standard initial value problem. By construction, the resulting solution complies with the algebraic constraint (B10) at any time $t \geq 0$.

[1] F. Giazotto, T. T. Heikkilä, A. Luukanen, A. M. Savin, and J. P. Pekola, Opportunities for mesoscopics in thermometry and refrigeration: Physics and applications, *Rev. Mod. Phys.* **78**, 217 (2006).

[2] N. Linden, S. Popescu, and P. Skrzypczyk, How Small Can Thermal Machines Be? The Smallest Possible Refrigerator, *Phys. Rev. Lett.* **105**, 130401 (2010).

- [3] J. T. Muhonen, M. Meschke, and J. P. Pekola, Micrometre-scale refrigerators, *Rep. Prog. Phys.* **75**, 046501 (2012).
- [4] H. Courtois, F. W. J. Hekking, H. Q. Nguyen, and C. B. Winkelmann, Electronic coolers based on superconducting tunnel junctions: Fundamentals and applications, *J. Low Temp. Phys.* **175**, 799 (2014).
- [5] J. P. Pekola, Towards quantum thermodynamics in electronic circuits, *Nat. Phys.* **11**, 118 (2015).
- [6] M. H. Devoret and R. J. Schoelkopf, Superconducting circuits for quantum information: An outlook, *Science* **339**, 1169 (2013).
- [7] R. Barends, J. Kelly, A. Megrant, A. Veitia, D. Sank, E. Jeffrey, T. C. White, J. Mutus, A. G. Fowler, B. Campbell, Y. Chen, Z. Chen, B. Chiaro, A. Dunsworth, C. Neill, P. O'Malley, P. Roushan, A. Vainsencher, J. Wenner, A. N. Korotkov *et al.*, Superconducting quantum circuits at the surface code threshold for fault tolerance, *Nature (London)* **508**, 500 (2014).
- [8] J. Kelly, R. Barends, A. G. Fowler, A. Megrant, E. Jeffrey, T. C. White, D. Sank, J. Y. Mutus, B. Campbell, Y. Chen, Z. Chen, B. Chiaro, A. Dunsworth, I.-C. Hoi, C. Neill, P. J. J. O'Malley, C. Quintana, P. Roushan, A. Vainsencher, J. Wenner *et al.*, State preservation by repetitive error detection in a superconducting quantum circuit, *Nature (London)* **519**, 66 (2015).
- [9] M. Grajcar, S. H. W. van der Ploeg, A. Izmalkov, E. Il'ichev, H.-G. Meyer, A. Fedorov, A. Shnirman, and G. Schön, Sisyphean cooling and amplification by a superconducting qubit, *Nat. Phys.* **4**, 612 (2008).
- [10] F. Giazotto and M. J. Martínez-Pérez, The Josephson heat interferometer, *Nature (London)* **492**, 401 (2012).
- [11] M. Partanen, K. Y. Tan, J. Govenius, R. E. Lake, M. K. Mäkelä, T. Tanttu, and M. Möttönen, Quantum-limited heat conduction over macroscopic distances, *Nat. Phys.* **12**, 460 (2016).
- [12] A. Fornieri, C. Blanc, R. Bosisio, S. D'Ambrosio, and F. Giazotto, Nanoscale phase engineering of thermal transport with a Josephson heat modulator, *Nat. Nanotechnol.* **11**, 258 (2016).
- [13] G. Marchegiani, P. Virtanen, F. Giazotto, and M. Campisi, Self-Oscillating Josephson Quantum Heat Engine, *Phys. Rev. Appl.* **6**, 054014 (2016).
- [14] P. P. Hofer, M. Perarnau-Llobet, J. B. Brask, R. Silva, M. Huber, and N. Brunner, Autonomous quantum refrigerator in a circuit QED architecture based on a Josephson junction, *Phys. Rev. B* **94**, 235420 (2016).
- [15] K. Y. Tan, M. Partanen, R. E. Lake, J. Govenius, S. Masuda, and M. Möttönen, Quantum-circuit refrigerator, *Nat. Commun.* **8**, 15189 (2017).
- [16] A. Ronzani, B. Karimi, J. Senior, Y.-C. Chang, J. T. Peltonen, C. Chen, and J. P. Pekola, Tunable photonic heat transport in a quantum heat valve, *Nat. Phys.* **14**, 991 (2018).
- [17] H. T. Quan, Y. D. Wang, Y.-x. Liu, C. P. Sun, and F. Nori, Maxwell's Demon Assisted Thermodynamic Cycle in Superconducting Quantum Circuits, *Phys. Rev. Lett.* **97**, 180402 (2006).
- [18] A. O. Niskanen, Y. Nakamura, and J. P. Pekola, Information entropic superconducting microcooler, *Phys. Rev. B* **76**, 174523 (2007).
- [19] A. E. Allahverdyan, K. Hovhannisyanyan, and G. Mahler, Optimal refrigerator, *Phys. Rev. E* **81**, 051129 (2010).
- [20] R. Kosloff and T. Feldmann, Optimal performance of reciprocating demagnetization quantum refrigerators, *Phys. Rev. E* **82**, 011134 (2010).
- [21] T. Feldmann and R. Kosloff, Short time cycles of purely quantum refrigerators, *Phys. Rev. E* **85**, 051114 (2012).
- [22] M. Kolář, D. Gelbwaser-Klimovsky, R. Alicki, and G. Kurizki, Quantum Bath Refrigeration Towards Absolute Zero: Challenging the Unattainability Principle, *Phys. Rev. Lett.* **109**, 090601 (2012).
- [23] Y. Izumida, K. Okuda, A. C. Hernández, and J. M. M. Roco, Coefficient of performance under optimized figure of merit in minimally nonlinear irreversible refrigerator, *Europhys. Lett.* **101**, 10005 (2013).
- [24] M. Campisi, J. Pekola, and R. Fazio, Nonequilibrium fluctuations in quantum heat engines: Theory, example, and possible solid state experiments, *New J. Phys.* **17**, 035012 (2015).
- [25] R. Uzdin, A. Levy, and R. Kosloff, Equivalence of Quantum Heat Machines, and Quantum-Thermodynamic Signatures, *Phys. Rev. X* **5**, 031044 (2015).
- [26] O. Abah and E. Lutz, Optimal performance of a quantum Otto refrigerator, *Europhys. Lett.* **113**, 60002 (2016).
- [27] K. Proesmans, Y. Dreher, M. Gavrilov, J. Bechhoefer, and C. Van den Broeck, Brownian Duet: A Novel Tale of Thermodynamic Efficiency, *Phys. Rev. X* **6**, 041010 (2016).
- [28] J. P. Pekola, B. Karimi, G. Thomas, and D. V. Averin, Supremacy of incoherent sudden cycles, [arXiv:1812.10933](https://arxiv.org/abs/1812.10933).
- [29] R. S. Whitney, Most Efficient Quantum Thermoelectric at Finite Power Output, *Phys. Rev. Lett.* **112**, 130601 (2014).
- [30] B. Sothmann, R. Sánchez, and A. N. Jordan, Thermoelectric energy harvesting with quantum dots, *Nanotechnology* **26**, 032001 (2014).
- [31] G. Benenti, G. Casati, K. Saito, and R. S. Whitney, Fundamental aspects of steady-state conversion of heat to work at the nanoscale, *Phys. Rep.* **694**, 1 (2017).
- [32] T. Schmiedl and U. Seifert, Efficiency at maximum power: An analytically solvable model for stochastic heat engines, *Europhys. Lett.* **81**, 20003 (2007).
- [33] M. Esposito, R. Kawai, K. Lindenberg, and C. V. den Broeck, Finite-time thermodynamics for a single-level quantum dot, *Europhys. Lett.* **89**, 20003 (2010).
- [34] B. Andresen, Current Trends in Finite-Time Thermodynamics, *Angew. Chem. Int. Ed.* **50**, 2690 (2011).
- [35] E. Aurell, C. Mejía-Monasterio, and P. Muratore-Ginanneschi, Optimal Protocols and Optimal Transport in Stochastic Thermodynamics, *Phys. Rev. Lett.* **106**, 250601 (2011).
- [36] D. A. Sivak and G. E. Crooks, Thermodynamic Metrics and Optimal Paths, *Phys. Rev. Lett.* **108**, 190602 (2012).
- [37] V. Holubec, An exactly solvable model of a stochastic heat engine: Optimization of power, power fluctuations and efficiency, *J. Stat. Mech.* (2014) P05022.
- [38] A. Dechant, N. Kiesel, and E. Lutz, All-Optical Nanomechanical Heat Engine, *Phys. Rev. Lett.* **114**, 183602 (2015).
- [39] K. Brandner, K. Saito, and U. Seifert, Thermodynamics of Micro- and Nano-Systems Driven by Periodic Temperature Variations, *Phys. Rev. X* **5**, 031019 (2015).
- [40] M. Bauer, K. Brandner, and U. Seifert, Optimal performance of periodically driven, stochastic heat engines under limited control, *Phys. Rev. E* **93**, 042112 (2016).

- [41] A. Dechant, N. Kiesel, and E. Lutz, Underdamped stochastic heat engine at maximum efficiency, *Europhys. Lett.* **119**, 50003 (2017).
- [42] A. P. Solon and J. M. Horowitz, Phase Transition in Protocols Minimizing Work Fluctuations, *Phys. Rev. Lett.* **120**, 180605 (2018).
- [43] R. Uzdin and R. Kosloff, Universal features in the efficiency at maximal work of hot quantum Otto engines, *Europhys. Lett.* **108**, 40001 (2014).
- [44] K. Brandner and U. Seifert, Periodic thermodynamics of open quantum systems, *Phys. Rev. E* **93**, 062134 (2016).
- [45] B. Karimi and J. P. Pekola, Otto refrigerator based on a superconducting qubit: Classical and quantum performance, *Phys. Rev. B* **94**, 184503 (2016).
- [46] N. Suri, F. C. Binder, B. Muralidharan, and S. Vinjanampathy, Speeding up thermalisation via open quantum system variational optimisation, *Eur. Phys. J. Spec. Top.* **227**, 203 (2018).
- [47] V. Cavina, A. Mari, A. Carlini, and V. Giovannetti, Optimal thermodynamic control in open quantum systems, *Phys. Rev. A* **98**, 012139 (2018).
- [48] P. A. Erdman, V. Cavina, R. Fazio, F. Taddei, and V. Giovannetti, Maximum power and corresponding efficiency for two-level quantum heat engines and refrigerators, [arXiv:1812.05089](https://arxiv.org/abs/1812.05089).
- [49] D. E. Kirk, *Optimal Control Theory: An Introduction* (Courier Corporation, North Chelmsford, MA, 2004).
- [50] F. Boldt, K. H. Hoffmann, P. Salamon, and R. Kosloff, Time-optimal processes for interacting spin systems, *Europhys. Lett.* **99**, 40002 (2012).
- [51] S. Deffner, Optimal control of a qubit in an optical cavity, *J. Phys. B* **47**, 145502 (2014).
- [52] R. Kosloff and Y. Rezek, The quantum harmonic Otto cycle, *Entropy* **19**, 136 (2017).
- [53] L. S. Pontryagin, V. G. Boltyanskii, R. V. Gamkrelidze, and E. F. Mishchenko, *The Mathematical Theory of Optimal Processes* (John Wiley and Sons, New York, 1962).
- [54] U. Seifert, Stochastic thermodynamics, fluctuation theorems and molecular machines, *Rep. Prog. Phys.* **75**, 126001 (2012).
- [55] D. Gelbwaser-Klimovsky, W. Niedenzu, and G. Kurizki, Thermodynamics of quantum systems under dynamical control, in *Advances in Atomic, Molecular, and Optical Physics*, edited by E. Arimondo, C. C. Lin, and S. F. Yelin (Academic, New York, 2015), Vol. 64, Chap. 12, pp. 329–407.
- [56] H. Spohn and J. L. Lebowitz, Irreversible thermodynamics for quantum systems weakly coupled to thermal reservoirs, in *Advances in Chemical Physics*, edited by S. A. Rice, Vol. 38 (John Wiley & Sons, Inc., 1978), p. 109.
- [57] R. Alicki, The quantum open system as a model of the heat engine, *J. Phys. A* **12**, L103 (1979).
- [58] E. Geva and R. Kosloff, Three-level quantum amplifier as a heat engine: A study in finite-time thermodynamics, *Phys. Rev. E* **49**, 3903 (1994).
- [59] S. Vinjanampathy and J. Anders, Quantum thermodynamics, *Contemp. Phys.* **57**, 545 (2016).
- [60] H. Goldstein, C. P. Poole, and J. L. Safko, *Classical Mechanics* (Addison Wesley, Reading, MA, 2002).
- [61] T. Schmiedl and U. Seifert, Optimal Finite-Time Processes In Stochastic Thermodynamics, *Phys. Rev. Lett.* **98**, 108301 (2007).
- [62] An alternative way to see that $\omega_i^q[\mathbf{R}_0, \lambda_0] = \omega_i^p[\mathbf{R}_0, \lambda_0]$ must hold during the work stroke is to observe that the protocol minimizing the effective input Q_h for fixed effective output Q_c^* simultaneously maximizes the output for fixed input.
- [63] U. Seifert, First and Second Law of Thermodynamics at Strong Coupling, *Phys. Rev. Lett.* **116**, 020601 (2016).
- [64] C. Jarzynski, Stochastic and Macroscopic Thermodynamics of Strongly Coupled Systems, *Phys. Rev. X* **7**, 011008 (2017).
- [65] R. S. Whitney, Non-Markovian quantum thermodynamics: Laws and fluctuation theorems, *Phys. Rev. B* **98**, 085415 (2018).
- [66] Note that we have rescaled the objective functional, giving the Lagrange multiplier the same dimension as ω .
- [67] Since the work stroke has a maximum duration, there are admissible initial conditions for which there is no intersection. We handle this case in practice by allowing for an intermediate time in which the system is decoupled from both reservoirs and the system state remains constant. We find that the protocol yielding the maximal average cooling power never decouples the system from both reservoirs.
- [68] C. Zhu, R. H. Byrd, P. Lu, and J. Nocedal, Algorithm 778: L-BFGS-B: Fortran subroutines for large-scale bound-constrained optimization, *ACM Trans. Math. Softw.* **23**, 550 (1997).
- [69] Note that, in order to account for reset protocols with $\omega_{\tau'} > \omega'$, τ_1 must be allowed to become smaller than τ' .
- [70] A. Ryabov and V. Holubec, Maximum efficiency of steady-state heat engines at arbitrary power, *Phys. Rev. E* **93**, 050101(R) (2016).
- [71] N. Shiraishi, K. Saito, and H. Tasaki, Universal Trade-Off Relation between Power and Efficiency for Heat Engines, *Phys. Rev. Lett.* **117**, 190601 (2016).
- [72] P. Pietzonka and U. Seifert, Universal Trade-Off between Power, Efficiency, and Constancy in Steady-State Heat Engines, *Phys. Rev. Lett.* **120**, 190602 (2018).
- [73] N. Shiraishi and K. Saito, Fundamental relation between entropy production and heat current, *J. Stat. Phys.* **174**, 433 (2019).
- [74] V. Cavina, A. Mari, and V. Giovannetti, Slow Dynamics and Thermodynamics of Open Quantum Systems, *Phys. Rev. Lett.* **119**, 050601 (2017).
- [75] We note that for the adiabatic approximation to apply here, the relaxation time $1/\gamma$ has to be large compared to both the cycle time τ and the time scale of the coherent oscillations.
- [76] H. T. Quan, Y. X. Liu, C. P. Sun, and F. Nori, Quantum thermodynamic cycles and quantum heat engines, *Phys. Rev. E* **76**, 031105 (2007).
- [77] R. Kosloff, Quantum thermodynamics: A dynamical viewpoint, *Entropy* **15**, 2100 (2013).
- [78] K. Brandner, M. Bauer, and U. Seifert, Universal Coherence-Induced Power Losses of Quantum Heat Engines in Linear Response, *Phys. Rev. Lett.* **119**, 170602 (2017).
- [79] V. Holubec and A. Ryabov, Cycling Tames Power Fluctuations Near Optimum Efficiency, *Phys. Rev. Lett.* **121**, 120601 (2018).
- [80] N. Brunner, M. Huber, N. Linden, S. Popescu, R. Silva, and P. Skrzypczyk, Entanglement enhances cooling in microscopic quantum refrigerators, *Phys. Rev. E* **89**, 032115 (2014).

- [81] J. Roßnagel, O. Abah, F. Schmidt-Kaler, K. Singer, and E. Lutz, Nanoscale Heat Engine Beyond the Carnot Limit, *Phys. Rev. Lett.* **112**, 030602 (2014).
- [82] M. Lostaglio, K. Korzekwa, D. Jennings, and T. Rudolph, Quantum Coherence, Time-Translation Symmetry, and Thermodynamics, *Phys. Rev. X* **5**, 021001 (2015).
- [83] P. Ćwikliński, M. Studziński, M. Horodecki, and J. Oppenheim, Limitations on the Evolution of Quantum Coherences: Towards Fully Quantum Second Laws of Thermodynamics, *Phys. Rev. Lett.* **115**, 210403 (2015).
- [84] J. Klaers, S. Faelt, A. Imamoglu, and E. Togan, Squeezed Thermal Reservoirs as a Resource for a Nanomechanical Engine beyond the Carnot Limit, *Phys. Rev. X* **7**, 031044 (2017).
- [85] R. Uzdin and S. Rahav, Global Passivity in Microscopic Thermodynamics, *Phys. Rev. X* **8**, 021064 (2018).
- [86] M. Kolodrubetz, D. Sels, P. Mehta, and A. Polkovnikov, Geometry and non-adiabatic response in quantum and classical systems, *Phys. Rep.* **697**, 1 (2017).
- [87] C. Jarzynski, Generating shortcuts to adiabaticity in quantum and classical dynamics, *Phys. Rev. A* **88**, 040101(R) (2013).
- [88] S. Deffner, C. Jarzynski, and A. del Campo, Classical and Quantum Shortcuts to Adiabaticity for Scale-Invariant Driving, *Phys. Rev. X* **4**, 021013 (2014).
- [89] S. Blanes, F. Casas, J. A. Oteo, and J. Ros, The Magnus expansion and some of its applications, *Phys. Rep.* **470**, 151 (2009).